



Shahid Chamran
University of Ahvaz

Journal of Applied and Computational Mechanics



Research Paper

Modeling of Turbulent Two-Phase Flow based on a Two-Fluid Approach

Z.M. Malikov¹, M.E. Madaliev^{1,2}

¹ Institute of Mechanics and Seismic Stability of Structures Named after M.T. Urazbaev Academy of Sciences of the Republic of Uzbekistan, 100125, Durmon yuli st. 33, Tashkent, Uzbekistan, Email: malikov.z62@mail.ru

² Fergana Polytechnic Institute Fergana, 150107 Fergana, st. Fergana, 86, Uzbekistan, Email: Madaliev.me2019@mail.ru, m.e.madaliev@ferpi.uz

Received May 18 2024; Revised June 25 2024; Accepted for publication July 02 2024.

Corresponding author: M.E. Madaliev (Madaliev.me2019@mail.ru; m.e.madaliev@ferpi.uz)

© 2024 Published by Shahid Chamran University of Ahvaz

Abstract. The paper presents the modeling of two-phase flow in turbulent flow. For this purpose, a two-fluid turbulence model is used. The work can be considered the development of a two-fluid approach to the problem of turbulence, which, unlike Reynolds' approach, leads to a closed system of equations. Therefore, the system of equations for a two-phase flow given in the work based on the two-fluid approach is also closed and no additional hypotheses are required. The resulting system of equations for a turbulent two-phase flow is implemented numerically for a two-phase flow in a cylindrical pipe and in a free jet. The obtained results are compared with known experimental data, as well as with the results of the Reynolds stress method (RSM). The results of the proposed model are in good agreement with experimental data. In addition, it is shown that the model adequately describes the phenomenon of "turbulent migration of particles," resulting in the accumulation of inertial particles on the axis and wall of the pipe.

Keywords: Two-fluid model, turbulent particle transport, two-phase flow in a pipe, two-phase jet.

1. Introduction

Turbulent two-phase flow modeling is an important area of research in fluid mechanics. It plays a key role in understanding and analyzing the behavior of various processes, including mixing, heat transfer, aerodynamics and transport phenomena in applications ranging from industrial processes to natural phenomena in the environment [1, 2]. Turbulent two-phase flows are characterized by complex interactions between two or more phases, such as liquid-gas, liquid-liquid, or gas-solid. These flows are often found in a wide range of applications such as process technology, oil and gas industries, aerospace engineering, river hydraulics and soil remediation. A large number of experimental and numerical studies have been devoted to studying the transfer of aerosol particles and droplets in a turbulent flow [3–8]. In addition to its fundamental significance, the process of particle transfer in turbulent flows is also of great practical importance. Because in many technological processes the working environment is precisely multiphase turbulent flows. Multiphase flows are used in the oil and gas industry, in hydraulic engineering, when transporting oil and gas and gas condensate mixtures through pipelines [9]. Despite many years of research in this area, there are still many unresolved problems. The main problem is due to the fact that the question of turbulence, even for a single-phase flow, has not yet received a final answer. Indeed, if you look at the history of the development of mathematical models of turbulent flows, it is easy to notice that the overwhelming majority of them are based on time-averaged Reynolds equations with various methods of their closure, focused on fairly narrow classes of flows and significantly based on experimental data [10–15]. Therefore, "rough empiricism" still prevails for modeling multiphase flows. This applies to the greatest extent to vapor-liquid flows. Unlike single-phase hydrodynamics, where it is generally accepted that the Navier-Stokes system of equations is sufficient to describe the entire variety of flows, such a generally accepted mathematical model does not yet exist for vapor-liquid flows. Things are much better in the field of mathematical modeling of two-phase flows, when one of the phases is solid particles or aerosols [16].

Several approaches have been proposed to simulate the influence of the dispersed phase on the turbulent characteristics of the continuous phase. The most common among them are the procedure for obtaining particle-related source terms by Reynolds averaging, which takes into account the suppression of turbulent energy due to additional dissipation, and the energy balance approach [17, 18], which allows taking into account turbulization of the flow due to the formation of a wake behind a large particle. In [19, 20], a comparative analysis of these two approaches was performed and it was shown that the first of them is apparently preferable for modeling two-phase turbulent flows with small particles, and the second, on the contrary, for flows with large particles.



The goal of modeling turbulent two-phase flows is to develop mathematical models that can accurately describe and predict the behavior of flow processes. This allows not only to better understand physical phenomena, but also to optimize technological processes, increase the efficiency and safety of various systems. This paper presents a mathematical model of a two-phase turbulent flow based on the two-fluid turbulence model of one of the authors [21]. The advantage of the two-fluid approach in modeling turbulence is that, unlike the Reynolds approach, it leads to a closed system of equations and has high accuracy, stability, and the ability to describe anisotropic turbulence. Therefore, the use of a two-fluid approach to modeling a two-phase turbulent flow also leads to a closed system of equations. In operation, the carrier phase is liquid, and the second phase is solid inclusions (particles). It has been shown that the presented two-phase turbulent flow model is capable of adequately describing a vertical turbulent two-phase jet flow [22–25], a vertical gas flow with solid particles in a pipe [26, 27], as well as a vertical liquid flow with solid particles in a pipe [28].

Therefore, the goal of this work is to construct a model of two-phase turbulent flow on a more rigorous mathematical basis. Several assumptions are made in the work: 1) The volume fraction of the solid phase in the elementary volume is considered small, therefore, the interaction between particles of the solid phase is neglected; 2) there are no phase transitions.

2. Description of a Two-Fluid Approach for Modeling of Turbulent Two-Phase Flow

In our previous work [21], we proposed a two-fluid approach to describe the turbulent flow. The essence of this approach is that turbulence can be represented as a heterogeneous mixture of two fluids, which have different velocities V_{1i}, V_{2i} and density equal ρ . Generalizing this approach to modeling a turbulent two-phase flow, we denote the velocities of solid inclusions in the first and second fluids for k -fraction by V_{p1ki}, V_{p2ki} and the relative mass concentrations of particles, respectively, by C_{1k}, C_{2k} . Let us write down the equations of the law of conservation of mass and momentum for the carrier and solid phases:

$$\frac{\partial \varepsilon \rho}{\partial t} + \frac{\partial \rho \alpha_j V_{1j}}{\partial x_j} = J, \quad (1a)$$

$$\frac{\partial (1 - \varepsilon) \rho}{\partial t} + \frac{\partial (1 - \alpha_j) \rho V_{2j}}{\partial x_j} = -J. \quad (1b)$$

$$\frac{\partial \varepsilon \rho V_{1i}}{\partial t} + \frac{\partial \alpha_j \rho V_{1j} V_{1i}}{\partial x_j} + \frac{\partial \alpha_j p}{\partial x_i} = \frac{\partial}{\partial x_j} \left[\alpha_j \rho \nu \left(\frac{\partial V_{1i}}{\partial x_j} + \frac{\partial V_{1j}}{\partial x_i} \right) \right] + J V_{1i} + \sum_{k=1}^N \varepsilon \rho C_{1k} (V_{p1ki} - V_{1i}) / \tau_{pk} + f_i, \quad (1c)$$

$$\frac{\partial (1 - \varepsilon) \rho V_{2i}}{\partial t} + \frac{\partial (1 - \alpha_j) \rho V_{2j} V_{2i}}{\partial x_j} + \frac{\partial (1 - \alpha_j) p}{\partial x_i} = \frac{\partial}{\partial x_j} \left[(1 - \alpha_j) \rho \nu \left(\frac{\partial V_{2i}}{\partial x_j} + \frac{\partial V_{2j}}{\partial x_i} \right) \right] - J V_{2i} + \sum_{k=1}^N (1 - \varepsilon) \rho C_{2k} (V_{p2ki} - V_{2i}) / \tau_{pk} - f_i. \quad (1d)$$

$$\frac{\partial \varepsilon \rho C_{1k}}{\partial t} + \frac{\partial \rho C_{1k} \alpha_j V_{p1j}}{\partial x_j} = J_p + \frac{\partial}{\partial x_j} (\alpha_j \rho D \frac{\partial C_{1k}}{\partial x_j}), \quad (1e)$$

$$\frac{\partial (1 - \varepsilon) \rho C_{2k}}{\partial t} + \frac{\partial (1 - \alpha_j) \rho C_{2k} V_{p2j}}{\partial x_j} = -J_p + \frac{\partial}{\partial x_j} ((1 - \alpha_j) \rho D \frac{\partial C_{2k}}{\partial x_j}). \quad (1f)$$

$$\frac{\partial V_{p1ki}}{\partial t} + V_{p1kj} \frac{\partial V_{p1ki}}{\partial x_j} = (V_{1i} - V_{p1ki}) / \tau_{pk}, \quad (1g)$$

$$\frac{\partial V_{p2ki}}{\partial t} + V_{p2kj} \frac{\partial V_{p2ki}}{\partial x_j} = (V_{2i} - V_{p2ki}) / \tau_{pk}. \quad (1h)$$

In the system of Eqs. (1), ε - the volume fraction of the first fluid in an elementary volume, α_j - the surface fraction of the first fluid in an elementary area in the j direction, p - the static pressure in the flow, J - the intensity of mass transfer of the carrier phase between two fluids, f_i - the interaction force per unit volume between two fluids, τ_{pk} - relaxation time of interaction between the carrier and solid phases, J_p - intensity of mass transfer of the solid phase of two fluids, D - diffusion coefficient of particles. In [21], it was shown that the averaged values of the volume and surface fractions are equal as follows:

$$\bar{\varepsilon} = \bar{\alpha}_i = 0.5.$$

Therefore, after averaging over time, we obtain a system of equations:

$$\frac{\partial \rho}{\partial t} + \frac{\partial \rho V_{1j}}{\partial x_j} = 2\bar{J}, \quad (2a)$$

$$\frac{\partial \rho}{\partial t} + \frac{\partial \rho V_{2j}}{\partial x_j} = -2\bar{J}. \quad (2b)$$

$$\frac{\partial \rho V_{1i}}{\partial t} + \frac{\partial \rho V_{1j} V_{1i}}{\partial x_j} + \frac{\partial p}{\partial x_i} = \frac{\partial}{\partial x_j} \left[\rho \nu \left(\frac{\partial V_{1i}}{\partial x_j} + \frac{\partial V_{1j}}{\partial x_i} \right) \right] + \bar{J} (V_{1i} + V_{2i}) + \sum_{k=1}^N \rho C_{1k} (V_{p1ki} - V_{1i}) / \tau_{pk} + 2\bar{f}_i, \quad (2c)$$

$$\frac{\partial \rho V_{2i}}{\partial t} + \frac{\partial \rho V_{2j} V_{2i}}{\partial x_j} + \frac{\partial p}{\partial x_i} = \frac{\partial}{\partial x_j} \left[\rho \nu \left(\frac{\partial V_{2i}}{\partial x_j} + \frac{\partial V_{2j}}{\partial x_i} \right) \right] - \bar{J} (V_{1i} + V_{2i}) + \sum_{k=1}^N \rho C_{2k} (V_{p2ki} - V_{2i}) / \tau_{pk} - 2\bar{f}_i. \quad (2d)$$



$$\frac{\partial \rho C_{1k}}{\partial t} + \frac{\partial \rho C_{1k} V_{p1j}}{\partial x_j} = 2\bar{J}_p + \frac{\partial}{\partial x_j} (\rho D \frac{\partial C_{1k}}{\partial x_j}), \quad (2e)$$

$$\frac{\partial \rho C_{2k}}{\partial t} + \frac{\partial \rho C_{2k} V_{p2j}}{\partial x_j} = -2\bar{J}_p + \frac{\partial}{\partial x_j} (\rho D \frac{\partial C_{2k}}{\partial x_j}). \quad (2f)$$

$$\frac{\partial V_{p1ki}}{\partial t} + V_{p1kj} \frac{\partial V_{p1ki}}{\partial x_j} = (V_{1i} - V_{p1ki}) / \tau_{pk}, \quad (2g)$$

$$\frac{\partial V_{p2ki}}{\partial t} + V_{p2kj} \frac{\partial V_{p2ki}}{\partial x_j} = (V_{2i} - V_{p2ki}) / \tau_{pk}. \quad (2h)$$

Here, \bar{J} , \bar{J}_p , \bar{f}_i , \bar{f}_{pi} are averaged values. For convenience, we introduce new variables as:

$$V_{1i} = V_i + \vartheta_i, \quad V_{2i} = V_i - \vartheta_i, \quad V_{p1ki} = V_{pki} + \vartheta_{pki}, \quad V_{p2ki} = V_{pki} - \vartheta_{pki}, \quad C_{1k} = C_k + c_k, \quad C_{2k} = C_k - c_k. \quad (3)$$

Here V_i, V_{pki}, C_k are the average velocities of the carrier and solid phases, as well as the mass concentration of the solid phase, $\vartheta_i, \vartheta_{pki}, c_k$ their relative values.

Substituting expressions (3) into system (2), after simple mathematical operations, we obtain a system of equations:

$$\frac{\partial \rho}{\partial t} + \frac{\partial \rho V_j}{\partial x_j} = 0, \quad (4a)$$

$$\frac{\partial \rho \vartheta_j}{\partial x_j} = 2\bar{J}. \quad (4b)$$

$$\frac{\partial \rho V_i}{\partial t} + \frac{\partial \rho V_j V_i}{\partial x_j} + \frac{\partial p}{\partial x_i} = \frac{\partial}{\partial x_j} \left[\rho \nu \left(\frac{\partial V_i}{\partial x_j} + \frac{\partial V_j}{\partial x_i} \right) - \rho \vartheta_j \vartheta_i \right] + \sum_{k=1}^N \rho C_k (V_{pki} - V_i) / \tau_{pk} + \sum_{k=1}^N \rho c_k (\vartheta_{pki} - \vartheta_i) / \tau_{pk}, \quad (4c)$$

$$\frac{\partial \rho \vartheta_i}{\partial t} + \frac{\partial \rho V_j \vartheta_i}{\partial x_j} + \rho \vartheta_j \frac{\partial V_i}{\partial x_j} = \frac{\partial}{\partial x_j} \left[\rho \nu \left(\frac{\partial \vartheta_i}{\partial x_j} + \frac{\partial \vartheta_j}{\partial x_i} \right) \right] + \sum_{k=1}^N \rho C_k (\vartheta_{pki} - \vartheta_i) / \tau_{pk} + \sum_{k=1}^N \rho c_k (V_{pki} - V_i) / \tau_{pk} + 2\bar{f}_i. \quad (4d)$$

$$\frac{\partial \rho C_k}{\partial t} + \frac{\partial \rho C_k V_{pkj}}{\partial x_j} + \frac{\partial c_k \vartheta_{pkj}}{\partial x_j} = \frac{\partial}{\partial x_j} (\rho D \frac{\partial C_k}{\partial x_j}), \quad (4e)$$

$$\frac{\partial \rho c_k}{\partial t} + \frac{\partial \rho c_k \vartheta_{pkj}}{\partial x_j} + \frac{\partial \rho c_k V_{pkj}}{\partial x_j} = 2\bar{J}_p + \frac{\partial}{\partial x_j} (\rho D \frac{\partial c_k}{\partial x_j}). \quad (4f)$$

$$\frac{\partial V_{pki}}{\partial t} + V_{pkj} \frac{\partial V_{pki}}{\partial x_j} + \vartheta_{pkj} \frac{\partial \vartheta_{pki}}{\partial x_j} = (V_i - V_{pki}) / \tau_{pk}, \quad (4g)$$

$$\frac{\partial \vartheta_{pki}}{\partial t} + V_{pkj} \frac{\partial \vartheta_{pki}}{\partial x_j} + \vartheta_{pkj} \frac{\partial V_{pki}}{\partial x_j} = (\vartheta_i - \vartheta_{pki}) / \tau_{pk}. \quad (4h)$$

Boulet and Moissette [21] provided a detailed analysis of the interaction force \bar{f}_i . Therefore, here we give an expression for this force:

$$\bar{f}_i = F_{si} + F_{fi} + \frac{\partial}{\partial x_j} \left[\rho \nu_{ji} \left(\frac{\partial \vartheta_i}{\partial x_j} + \frac{\partial \vartheta_j}{\partial x_i} \right) \right]$$

where,

$$\nu_{ji} = 2\nu + 2 \frac{\vartheta_i \vartheta_j}{\mathbf{def}(V)} \quad \text{if } i \neq j, \quad \nu_{ii} = 2\nu + \frac{2 \sum_{q=1}^3 \vartheta_q \vartheta_q \frac{\partial \vartheta_q}{\partial x_q}}{\mathbf{def}(V) \sum_{q=1}^3 \left| \frac{\partial \vartheta_q}{\partial x_q} \right|} \quad (5a)$$

$$F_{fi} = -K_f \vartheta_i, \quad F_{si} = C_s \mathbf{rot}(\vec{V} \times \vec{\vartheta})_i, \quad \mathbf{def}(V) = \sqrt{2S_{ij} S_{ij}}, \quad S_{ij} = \frac{1}{2} \left(\frac{\partial V_i}{\partial x_j} + \frac{\partial V_j}{\partial x_i} \right) \quad (5b)$$

Here ν_{ji} are the molecular kinematic viscosity, F_{si} is the perpendicular force component (Seffman force), F_{fi} is the friction force component, S_{ij} denotes the strain rate. In [21], it was shown that:

$$K_f = C_{f1} \lambda_{\max} + C_{f2} \frac{|\vec{d} \cdot \vec{\vartheta}|}{d^2},$$

where d is the closest distance from a given point to a solid wall and λ_{\max} is the largest root of the characteristic equation:

$$\det(A - \lambda E) = 0.$$



Here A is the following matrix:

$$A = \begin{pmatrix} -\frac{\partial V_1}{\partial x_1} & -\frac{\partial V_1}{\partial x_2} - C_s \zeta_3 & -\frac{\partial V_1}{\partial x_3} + C_s \zeta_2 \\ -\frac{\partial V_2}{\partial x_1} + C_s \zeta_3 & -\frac{\partial V_2}{\partial x_2} & -\frac{\partial V_2}{\partial x_3} - C_s \zeta_1 \\ -\frac{\partial V_3}{\partial x_1} - C_s \zeta_2 & -\frac{\partial V_3}{\partial x_2} + C_s \zeta_1 & -\frac{\partial V_3}{\partial x_3} \end{pmatrix}$$

and

$$\vec{\zeta} = \mathbf{rot} \vec{V}$$

Using a similar technique as in [21, 29], we define:

$$2\bar{J}_p = C_k \frac{\partial \rho \vartheta_{pkj}}{\partial x_j} + \frac{\partial}{\partial x_j} \left(\rho D_{pj} \frac{\partial C_k}{\partial x_j} \right) - \rho K_p C_k, \tag{6a}$$

$$D_{pj} = 2D + 2 \frac{|C_k \vartheta_{pkj}|}{|\mathbf{grad}(C_k)|}, \quad K_p = C_{p1} \lambda_{\max} \tag{6b}$$

In expressions (6), D_{pj} is the coefficient of molar diffusion, K_p is the coefficient of mass transfer due to the difference in mass concentration between the solid phases in the first and second fluids.

Substituting the resulting expressions into Eq. (4), we obtain the final system of equations for a turbulent two-phase flow based on the two-fluid approach:

$$\frac{\partial \rho}{\partial t} + \frac{\partial \rho V_j}{\partial x_j} = 0, \tag{7a}$$

$$\frac{\partial \rho V_i}{\partial t} + \frac{\partial \rho V_j V_i}{\partial x_j} + \frac{\partial p}{\partial x_i} = \frac{\partial}{\partial x_j} \left[\rho \nu \left(\frac{\partial V_i}{\partial x_j} + \frac{\partial V_j}{\partial x_i} \right) - \rho \vartheta_j \vartheta_i \right] + \sum_{k=1}^N \rho C_k (V_{pki} - V_i) / \tau_{pk} + \sum_{k=1}^N \rho c_k (\vartheta_{pki} - \vartheta_i) / \tau_{pk}, \tag{7b}$$

$$\frac{\partial \rho \vartheta_i}{\partial t} + \frac{\partial \rho V_j \vartheta_i}{\partial x_j} + \rho \vartheta_j \frac{\partial V_i}{\partial x_j} = F_{fi} + F_{si} + \frac{\partial}{\partial x_j} \left[\rho \nu_{ij} \left(\frac{\partial \vartheta_i}{\partial x_j} + \frac{\partial \vartheta_j}{\partial x_i} \right) \right] + \sum_{k=1}^N \rho C_k (\vartheta_{pki} - \vartheta_i) / \tau_{pk} + \sum_{k=1}^N \rho c_k (V_{pki} - V_i) / \tau_{pk} - K_f \vartheta_i. \tag{7c}$$

$$\frac{\partial \rho C_k}{\partial t} + \frac{\partial \rho C_k V_{pkj}}{\partial x_j} + \frac{\partial c_k \vartheta_{pkj}}{\partial x_j} = \frac{\partial}{\partial x_j} (\rho D_{pj} \frac{\partial C_k}{\partial x_j}), \tag{7d}$$

$$\frac{\partial \rho c_k}{\partial t} + \frac{\partial \rho c_k V_{pkj}}{\partial x_j} + \rho \vartheta_{pkj} \frac{\partial C_k}{\partial x_j} = \frac{\partial}{\partial x_j} (\rho D_{pj} \frac{\partial c_k}{\partial x_j}). \tag{7e}$$

$$\frac{\partial V_{pki}}{\partial t} + V_{pkj} \frac{\partial V_{pki}}{\partial x_j} + \vartheta_{pkj} \frac{\partial \vartheta_{pki}}{\partial x_j} = (V_i - V_{pki}) / \tau_{pk}, \tag{7f}$$

$$\frac{\partial \vartheta_{pki}}{\partial t} + V_{pkj} \frac{\partial \vartheta_{pki}}{\partial x_j} + \vartheta_{pkj} \frac{\partial V_{pki}}{\partial x_j} = (\vartheta_i - \vartheta_{pki}) / \tau_{pk}. \tag{7g}$$

$$\nu_{ji} = 3\nu + 2 \frac{|\vartheta_i \vartheta_j|}{|\mathbf{def}(V)|} \text{ if } i \neq j, \quad \nu_{ii} = 3\nu + \frac{2 \sum_{q=1}^3 \vartheta_q \vartheta_q \frac{\partial \vartheta_q}{\partial x_q}}{|\mathbf{def}(V)| \sum_{q=1}^3 \frac{|\partial \vartheta_q}{\partial x_q}|} \tag{7h}$$

$$F_{fi} = -K_f \vartheta_i, \quad F_{si} = C_s \mathbf{rot}(\vec{V} \times \vec{\vartheta})_i, \quad \mathbf{def}(V) = \sqrt{2S_{ij}S_{ij}}, \quad S_{ij} = \frac{1}{2} \left(\frac{\partial V_i}{\partial x_j} + \frac{\partial V_j}{\partial x_i} \right) \tag{7i}$$

$$D_{pj} = 2D + 2 \frac{|C_m \vartheta_{pj}|}{|\mathbf{grad}(C_m)|}, \quad K_p = C_{p1} \lambda_{\max}, \quad K_f = C_{f1} \lambda_{\max} + C_{f2} \frac{|\vec{d} \cdot \vec{\vartheta}|}{d^2}. \tag{7j}$$

The above works show that $C_s = 0.2$, $C_{f1} = 0.7825$, $C_{f2} = 0.306$, $C_{p1} = 0.915$. Below we consider problems of two-phase turbulent flow in an axisymmetric flow. Therefore, we write system (7) in a cylindrical coordinate system. Let us introduce the following notation:

$$x_1 = z, \quad x_2 = r, \quad V_1 = U, \quad V_2 = V, \quad \vartheta_1 = u, \quad \vartheta_2 = \vartheta, \quad V_{pk1} = U_p, \quad V_{pk2} = V_p, \quad \vartheta_{pk1} = u_p, \quad \vartheta_{pk2} = \vartheta_p. \tag{8a}$$



$$\nu_{zr} = \nu_{rz} = 3\nu + 2 \frac{u\vartheta}{|\mathbf{def}(\mathbf{V})|}, \quad \nu_{zz} = \nu_{rr} = 3\nu + \frac{2}{|\mathbf{def}(\mathbf{V})|} \cdot \frac{u^2 \left| \frac{\partial u}{\partial z} + \vartheta^2 \left| \frac{\partial r \vartheta}{r \partial r} \right|}{\left| \frac{\partial u}{\partial z} + \frac{\partial r \vartheta}{r \partial r} \right|} \quad (8b)$$

$$D_{pz} = 2D + 2 \frac{|c_m u_p|}{|\mathbf{grad}(C_m)|}, \quad D_{pr} = 2D + 2 \frac{|c_m \vartheta_p|}{|\mathbf{grad}(C_m)|}, \quad K_f = C_{f1} \lambda_{\max} + C_{f2} \frac{|\vec{d} \cdot \vec{\vartheta}|}{d^2}. \quad (8c)$$

$$\lambda_{\max} = \sqrt{C_s(1-C_s) \left[\frac{\partial V_r}{\partial z} - \frac{\partial V_z}{\partial r} \right]^2 + \frac{\partial V_r}{\partial z} \frac{\partial V_z}{\partial r} + \frac{1}{4} \left[\frac{\partial V_r}{\partial r} - \frac{\partial V_z}{\partial z} \right]^2} - \frac{1}{2} \left(\frac{\partial V_r}{\partial r} + \frac{\partial V_z}{\partial z} \right) \quad (8d)$$

The interaction relaxation time τ_p is determined as follows:

$$\tau_{pk} = \frac{4}{3\mu} \frac{\rho_p d_{pk}^2}{\text{Re}_p c_D}, \quad (9)$$

Here $\text{Re}_p = \frac{\rho |\mathbf{V} - \mathbf{V}_p| d_p}{\mu}$ denotes the Reynolds number for particles.

To determine the drag coefficient c_D , the standard empirical relation for a hard sphere was used [30]:

$$c_D = \begin{cases} 24 \text{Re}_p^{-1} (1 + 0.15 \text{Re}_p^{0.687}) & \text{Re}_p \leq 1000 \\ 0.44 & \text{Re}_p > 1000 \end{cases}. \quad (10)$$

3. Solution Method

Validation of systems of equations (8) was carried out for the flow of a vertical multiphase axisymmetric jet and for the flow in a vertical pipe. Numerical implementation of systems of equations (8) was carried out using an implicit finite-difference scheme. In the transverse direction, the central difference is used. To solve the implicit scheme, the sweep method was used. The integration steps for the jet were $\Delta z = 0.3$, $\Delta r = 0.1$, and for the problem of multiphase flow in a vertical pipe $\Delta z = 0.2$, $\Delta r = 0.01$, a staggered computational grid was used to match pressure with velocities. Velocity correction through pressure was carried out using the SIMPLE method [31]. Integration was carried out with a time step $\Delta t = 0.01$. Boundary conditions for adhesion were specified on all stationary solid walls for all velocities $V_z|_w = V_r|_w = \vartheta_z|_w = \vartheta_r|_w = V_{pz}|_w = V_{pr}|_w = \vartheta_{pz}|_w = \vartheta_{pr}|_w = 0$. At the exit from the channel, extrapolation conditions of the second order of accuracy were specified for all parameters.

Figure 1 shows a compute node. As mentioned above, the SIMPLE algorithm was used to solve the problems. As you can see in the picture, the variables are staggered. In the middle of the control volume there are pressures, concentration and relative velocities, and at the edges there are flow and particle velocities.

4. Vertical Turbulent Two-Phase Jet Flow

The two-phase flow (gas + solid particles) is considered, which exits from a pipe with a diameter of $d_1 = 13$ mm into a large pipe with a diameter of $d_2 = 60$ mm as shown in Fig. 2. More detailed information about the experimental setup is presented in the work of Hishida [22]. In the selected case, the velocity along the center line of the inner pipe was $U_1 = 30$ m/s, and the secondary flow velocity $U_2 = 15$ m/s. The average diameter of glass particles was $64.4 \mu\text{m}$, and the density $\rho = 2590$ kg/m³. The mass loading coefficient was 0.3 (kg particles)/(kg air), which corresponds to the average volume fraction $a_p = 1.4 \cdot 10^{-4}$. A comparison of measurements and calculations is discussed for sections at $x = 130$ and 260 mm after the nozzle, i.e. $x/d = 10$ and 20 [19].

The system of equations under consideration is reduced to dimensionless form. To do this, all dimensions are related to the radius $r_0 = d_1 / 2$ velocity to U_1 . At the input, experimental [22] profiles of averaged (Fig. 3a) and also fluctuating velocities for air and particles (Fig. 3b, Fig. 3c) were specified. The Reynolds number was equal to $\text{Re} = 4.2 \cdot 10^5$.

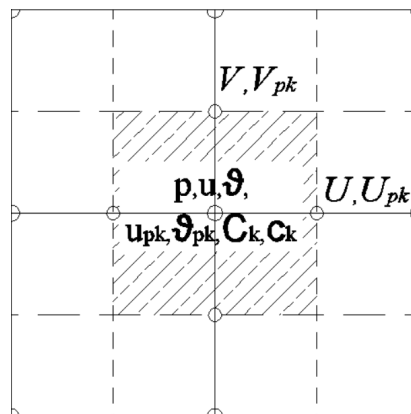


Fig. 1. Description of a compute node.



5. Calculation of the Results and Their Discussion

Figures 4 to 6 present the numerical results for air flow in sections $x/d_1 = 5, 10, 20$. In these figures, to demonstrate the effectiveness of the proposed turbulence model for two-phase flow, the results of the RSM model, which were obtained in [19], are also presented. Figure 4 shows the dimensionless axial flow velocity.

It is noted in [21, 29] that the two-fluid turbulence model describes flow velocities well. This trend can also be observed for two-phase flow. As can be seen from Fig. 4, the longitudinal air velocity according to the proposed model is in good agreement with the experimental results. As for the RSM model, it gives slightly overestimated values.

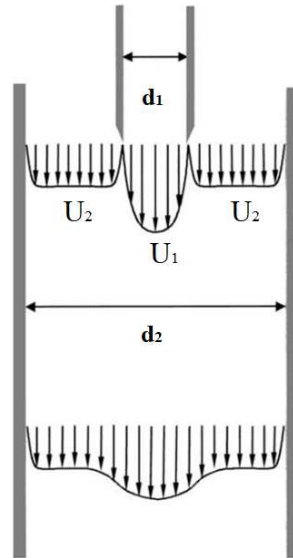


Fig. 2. Sketch of the jet stream configuration.

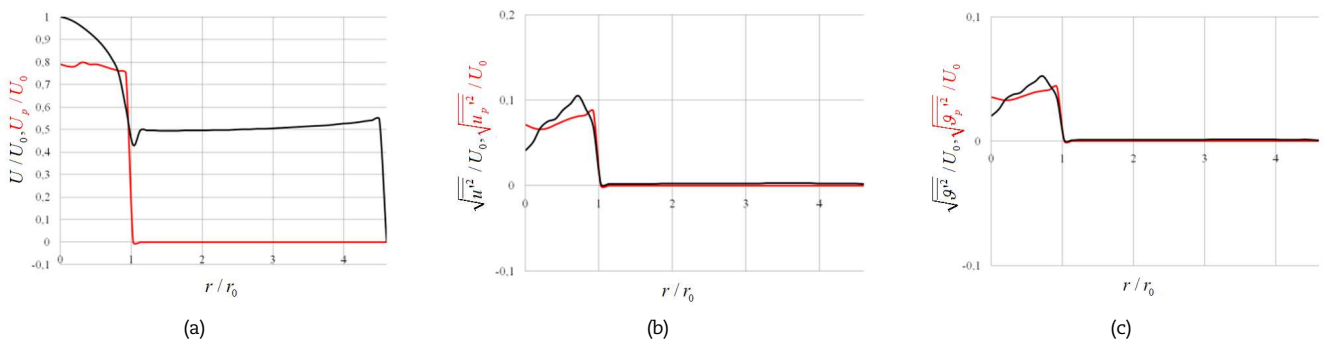


Fig. 3. Input data for the task.

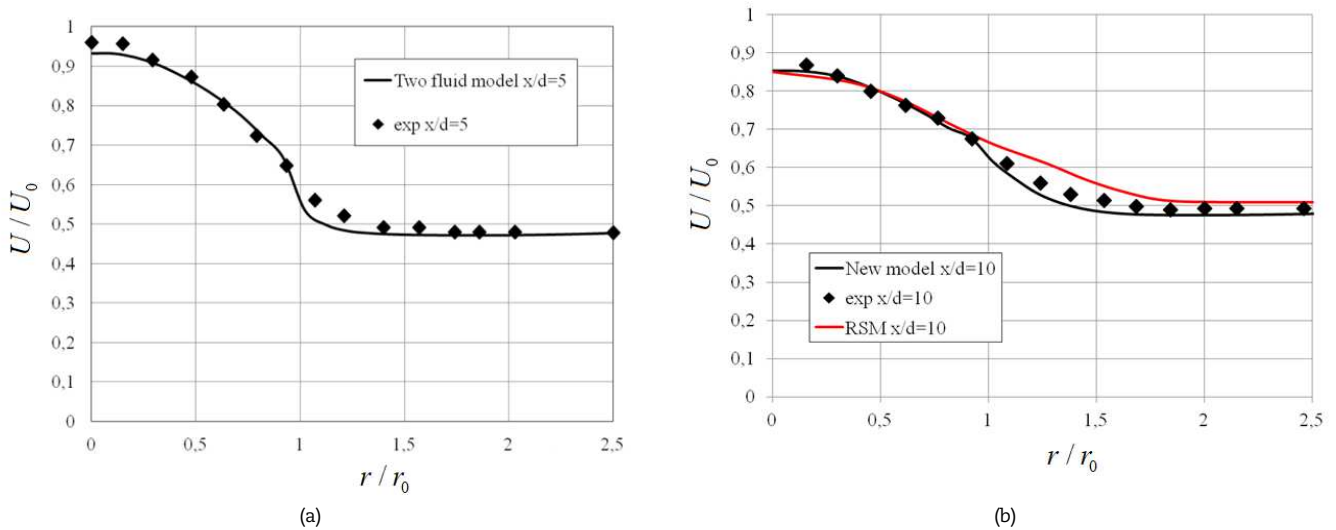


Fig. 4. Dimensionless axial flow velocity in different sections.



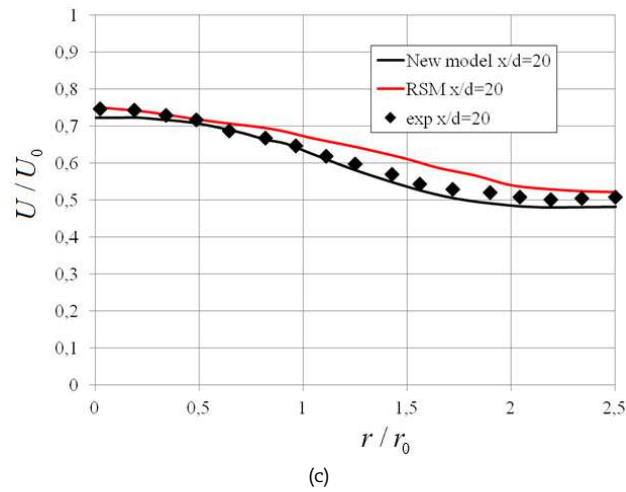


Fig. 4. Continued.

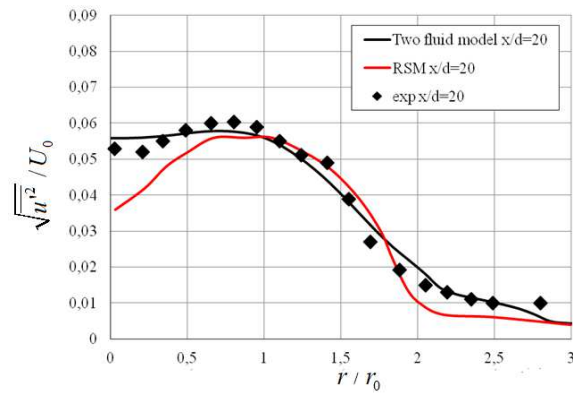
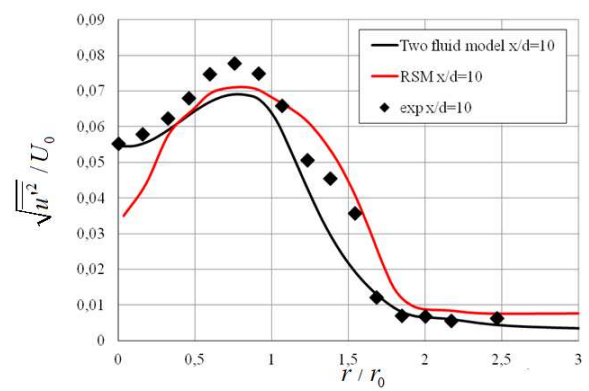
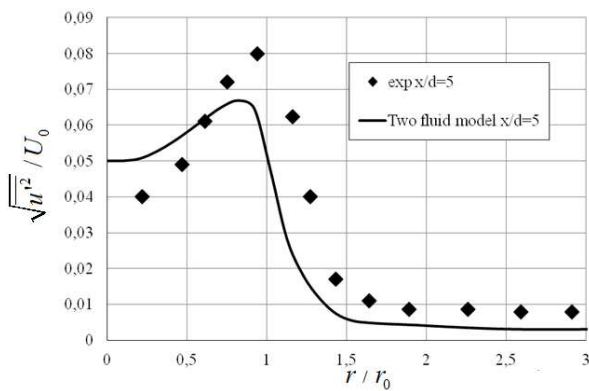


Fig. 5. Dimensionless axial fluctuating velocity of the gas phase.

Figures 5 to 6 show the dimensionless mean square fluctuation velocities for the gas phase ($\sqrt{u'^2}$ axial and $\sqrt{v'^2}$ radial). Averaged turbulent stresses are related to the parameters of the new turbulence model as follows:

$$\overline{\vartheta_i' \vartheta_j'} = \vartheta_i \vartheta_j + \frac{2}{3} k \delta_{ij} = \vartheta_i \vartheta_j + \frac{\delta_{ij}}{3} \sum_{m=1}^3 \vartheta_m^2$$

From here, we can determine the root-mean-square fluctuating velocities:

$$\sqrt{u'^2} = \sqrt{u^2 + \frac{2}{3} k} = \sqrt{u^2 + \frac{1}{3} (u^2 + \vartheta^2)}, \quad \sqrt{v'^2} = \sqrt{\vartheta^2 + \frac{2}{3} k} = \sqrt{\vartheta^2 + \frac{1}{3} (u^2 + \vartheta^2)}.$$

As can be seen from Fig. 5, the fluctuating axial air flow velocity according to the new model is in good agreement with the experimental data. Good agreement with experimental data is observed, especially far from the nozzle. Some discrepancy between the numerical results and the experimental data can be explained by the fact that the proposed model takes into account the interaction forces between two fluids, as well as between the fluid and the solid phase, only in a first approximation. Therefore, by refining these forces, it is possible to achieve even better agreement with experimental data.



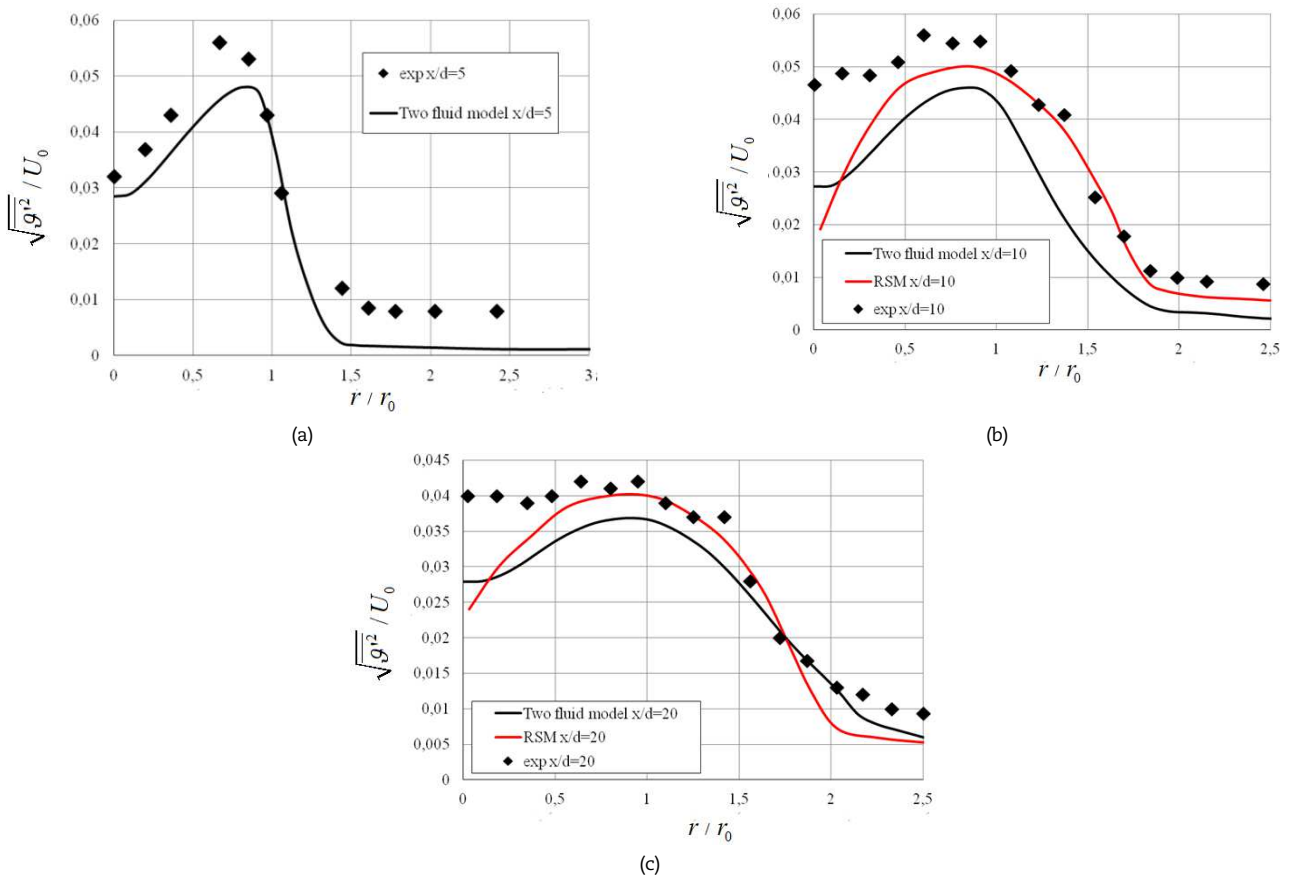


Fig. 6. Profiles of dimensionless fluctuating radial air flow velocity.

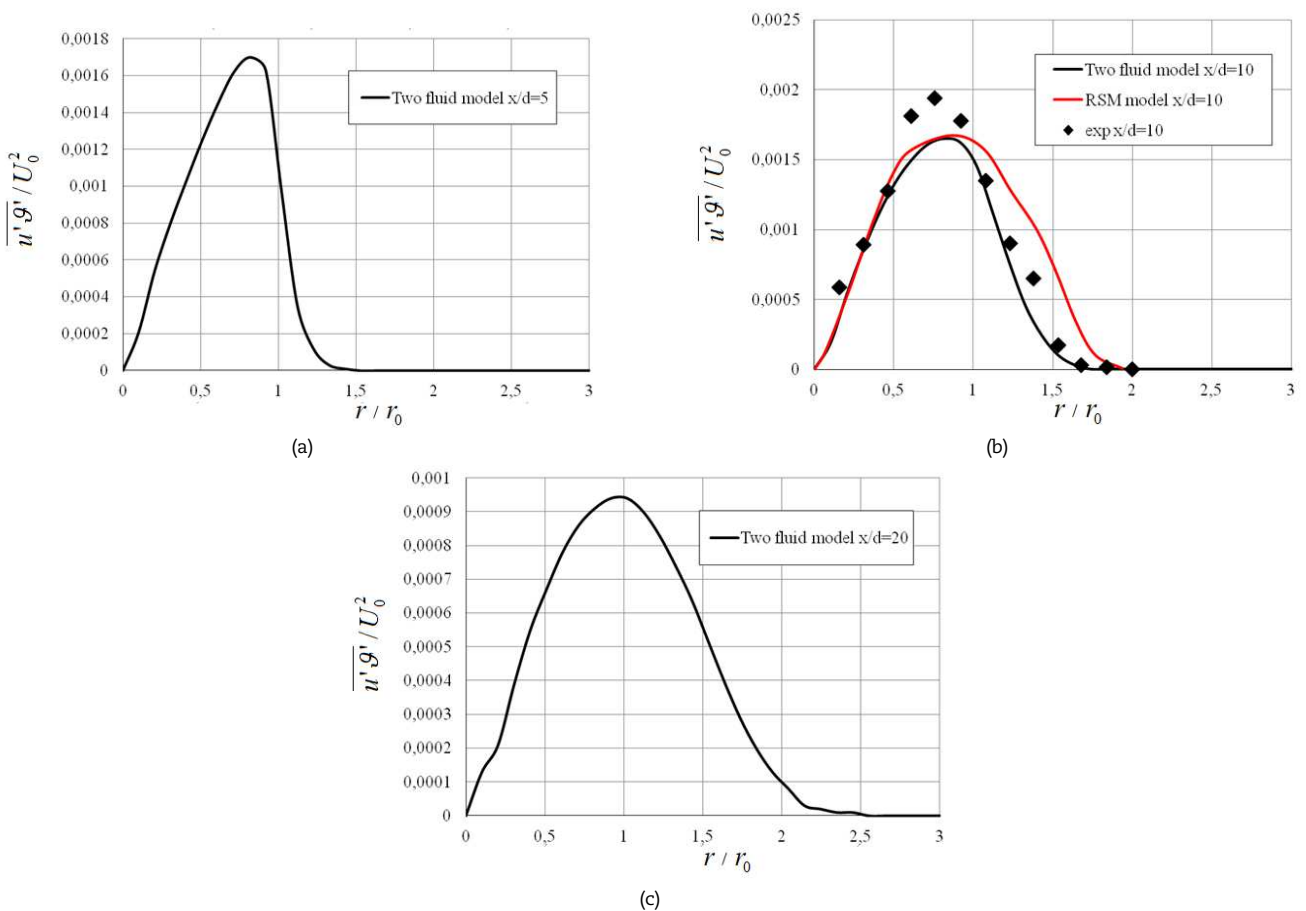


Fig. 7. Turbulent stress profiles for the gas phase.



Table 1. The relative error of mathematical models is in the area $x/d = 10$.

r/r_0	U					$\sqrt{u'^2}$				
	Two fluid model	RSM	exp	$\delta_{\text{Two fluid model}} \%$	$\delta_{\text{RSM}} \%$	Two fluid model	RSM	exp	$\delta_{\text{Two fluid model}} \%$	$\delta_{\text{RSM}} \%$
0	0,8622	0,8513	0,8826	2,04	3,13	0,05466	0,03334	0,05556	0,09	2,222
0,228	0,8481	0,8356	0,8591	1,1	2,35	0,0576	0,04819	0,0605	0,29	1,231
0,5	0,7876	0,7866	0,7886	0,1	0,2	0,06428	0,06578	0,0712	0,692	0,542
0,75	0,7213	0,737	0,7292	0,79	0,78	0,06924	0,0712	0,07827	0,903	0,707
1	0,6274	0,6744	0,6446	1,72	2,98	0,06428	0,06849	0,06774	0,346	0,075
1,24	0,5226	0,6149	0,5539	3,13	6,1	0,04187	0,06082	0,0506	0,873	1,022
1,5	0,4866	0,5617	0,5163	2,97	4,54	0,02112	0,045	0,0363	1,518	0,87
1,7	0,4787	0,5179	0,4959	1,72	2,2	0,0092	0,0149	0,01015	0,095	0,475
2	0,4787	0,5147	0,4959	1,72	1,88	0,0057	0,0089	0,00578	0,008	0,312
2,28	0,4772	0,5147	0,4959	1,87	1,88	0,0051	0,008	0,0065	0,14	0,15
2,5	0,4787	0,51	0,4944	1,57	1,56	0,0045	0,0078	0,006	0,15	0,18

It can be seen that the results of the new model for the radial fluctuating air flow velocity, as well as for the longitudinal one, deviate from the experiment in the area near the nozzle and approach the experiment as it moves away from the nozzle.

Figure 7 shows the dimensionless turbulent stress of the gas phase. In the experiment of Hishida [22], the turbulent stress value was measured only at $x/d = 10$. Therefore, in other sections only numerical results for stresses are presented.

It can be seen from the figure that the numerical results of the proposed model are in good agreement with the experimental data. To find out how close the result of the mathematical model is to the result of the experiment, it is necessary to present the results by section in the form of a table. In Table 1, the relative error of the flow velocity U and mean square fluctuation $\sqrt{u'^2}$ in the area $x/d = 10$ is described as a percentage. Here δ is the relative error in percentage.

As can be seen from Table 1, the flow rate at $x/d = 10$ shows an average relative error of 1.7% in the two-fluid model and 2.5% error in the RSM model. The velocity ripple has a relative error of 0.46% in the two-fluid model and 0.707% in the RSM model. These data indicate that the two-fluid model provides lower relative error for both flow rate and velocity fluctuation compared to the RSM model. Thus, for a given section $x/d = 10$ the two-fluid model seems to be more accurate and preferable compared to the RSM model.

It is known that searching for the particle velocity of a multiphase turbulent flow is of great importance. Therefore, Fig. 8 compares the axial velocity of particles with experimental results in different sections.

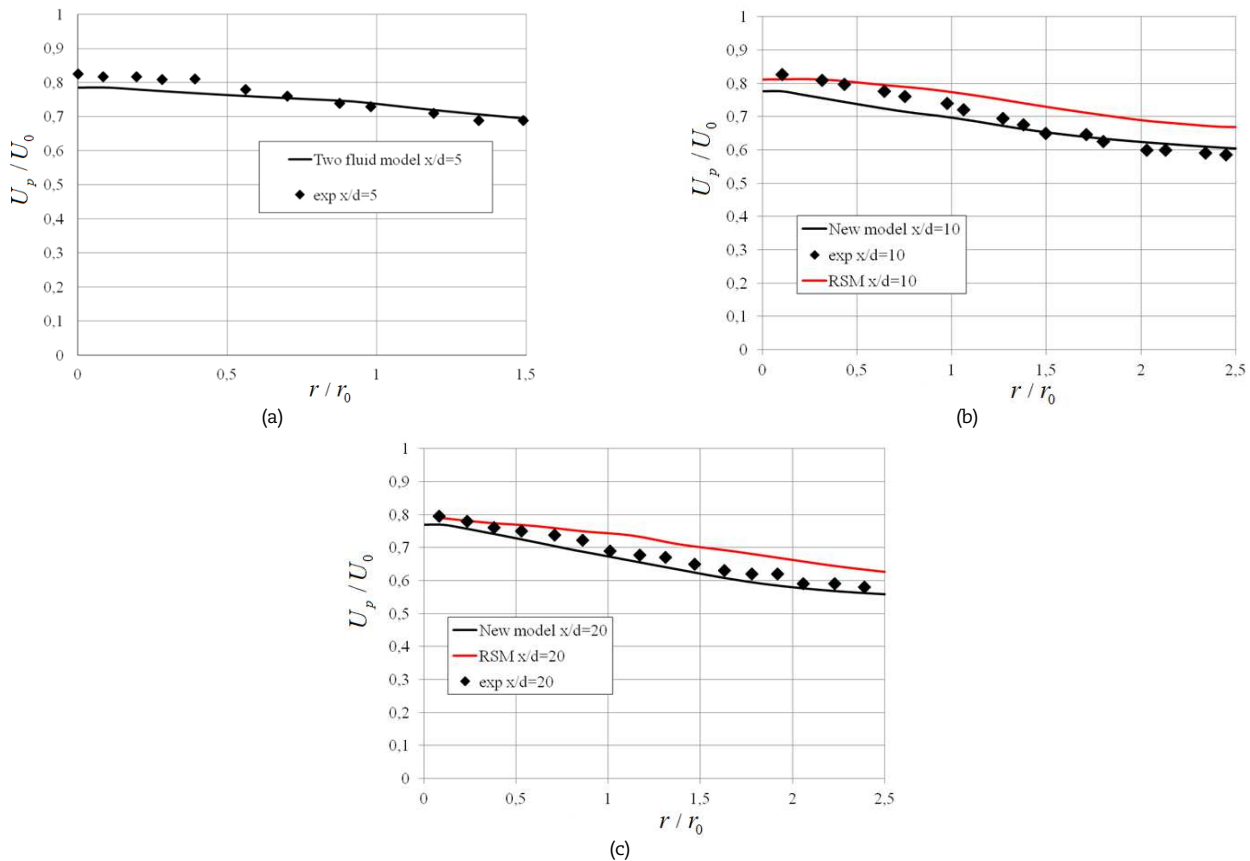


Fig. 8. Profiles of axial velocity of particles in various sections.



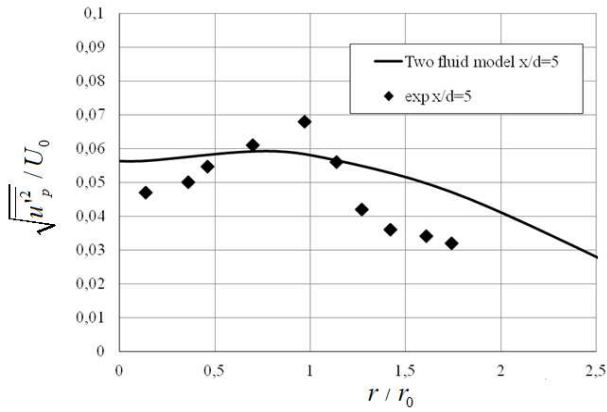


Fig. 9. Dimensionless axial fluctuating velocity of the solid phase.

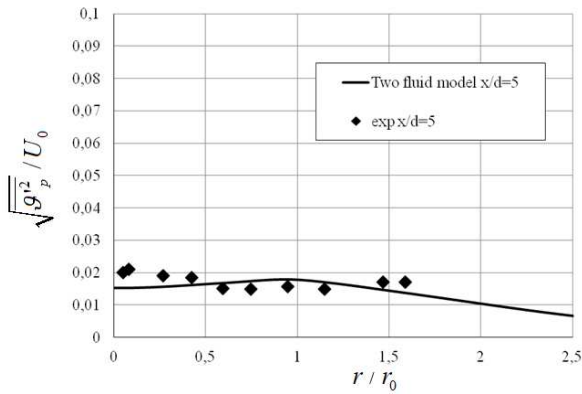
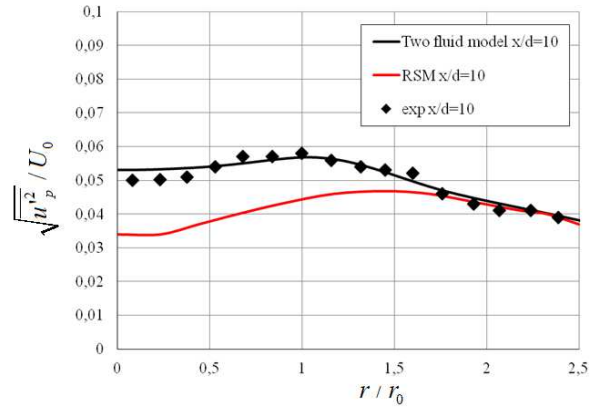


Fig. 10. Dimensionless radial fluctuating velocity of the solid phase.

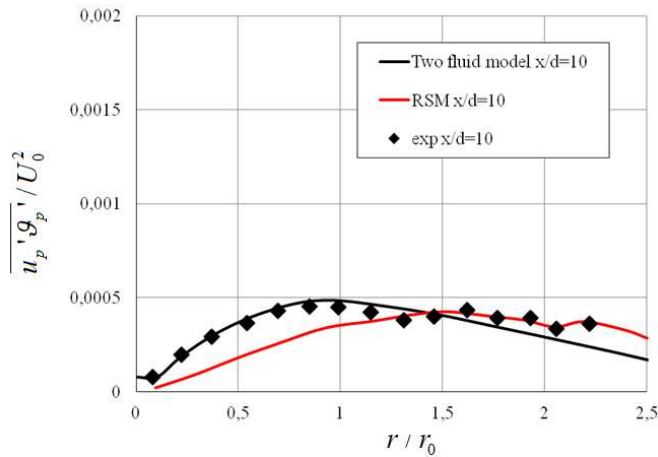
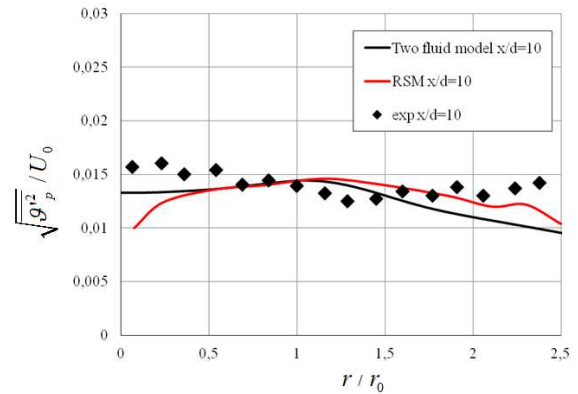


Fig. 11. Turbulent stress profile for the solid phase.

Figures 9 and 10 show the dimensionless fluctuating velocities of the solid phase ($\sqrt{u_p'^2}$ axial and $\sqrt{g_p'^2}$ radial). As can be seen from Figs. 9 and 10, the fluctuating velocities are in good agreement with the experimental results far from the nozzle. As noted above, the calculation results for fluctuating velocities can be improved by clarifying the interaction forces in the relative velocity equations. Figure 11 shows the turbulent stress for the solid phase.

This figure shows good agreement between the numerical results and the experimental data. Table 3 shows the relative errors of the particle velocity U_p and mean square fluctuation $\sqrt{u_p'^2}$ in the area $x/d = 10$.

As can be seen from Table 2, the particle velocity at $x/d = 10$ shows an average relative error of 3.2% in the two-fluid model and 5.06% in the RSM model. The fluctuation of velocities of particles has a relative error of 0.16% in the two-fluid model and 0.88% in the RSM model. These data indicate that the two-fluid model provides more accurate results for particles velocities and their fluctuations compared to the RSM model. The relative error of the two-fluid model is much lower, which makes it more preferable for modeling the behavior of particles in a turbulent two-phase flow. Figure 12 shows the contours of the averaged axial, fluctuating axial and radial velocities, as well as turbulent air tension. Figure 13 shows the contours for the solid phase parameters. Figure 14 shows isolines of concentration and turbulent flow for particles. As can be seen from Fig. 14, it is clear that particles accumulate away from the jet axis. This phenomenon is also observed in experimental observations.



Table 2. The relative error of mathematical models is in the area $x/d = 10$.

r/r_0	U_p					$\sqrt{u_p'^2}$				
	Two fluid model	RSM	exp	$\delta_{\text{Two fluid model}} \%$	$\delta_{\text{RSM}} \%$	Two fluid model	RSM	exp	$\delta_{\text{Two fluid model}} \%$	$\delta_{\text{RSM}} \%$
0	0,7785	0,8081	0,8315	5,3	2,34	0,05313	0,03383	0,0502	0,293	1,637
0,228	0,7644	0,8115	0,8143	4,99	0,28	0,05362	0,03367	0,04989	0,373	1,622
0,5	0,741	0,8065	0,7863	4,53	2,02	0,05459	0,03789	0,05329	0,13	1,54
0,75	0,7192	0,7909	0,7597	4,05	3,12	0,05621	0,0421	0,05881	0,26	1,671
1	0,6958	0,7769	0,7363	4,05	4,06	0,05686	0,04421	0,05848	0,162	1,427
1,24	0,6771	0,7535	0,7	2,29	5,35	0,05556	0,04648	0,05459	0,097	0,811
1,5	0,6521	0,7363	0,6552	0,31	8,11	0,05183	0,04697	0,05313	0,13	0,616
1,7	0,6381	0,7129	0,6537	1,56	5,92	0,04713	0,045	0,04648	0,065	0,148
2	0,6272	0,6864	0,6069	2,03	7,95	0,04437	0,04324	0,04194	0,243	0,13
2,28	0,6162	0,6771	0,596	2,02	8,11	0,04145	0,04032	0,04097	0,048	0,065
2,5	0,7785	0,8081	0,8315	5,3	2,34	0,05313	0,03383	0,0502	0,293	1,637

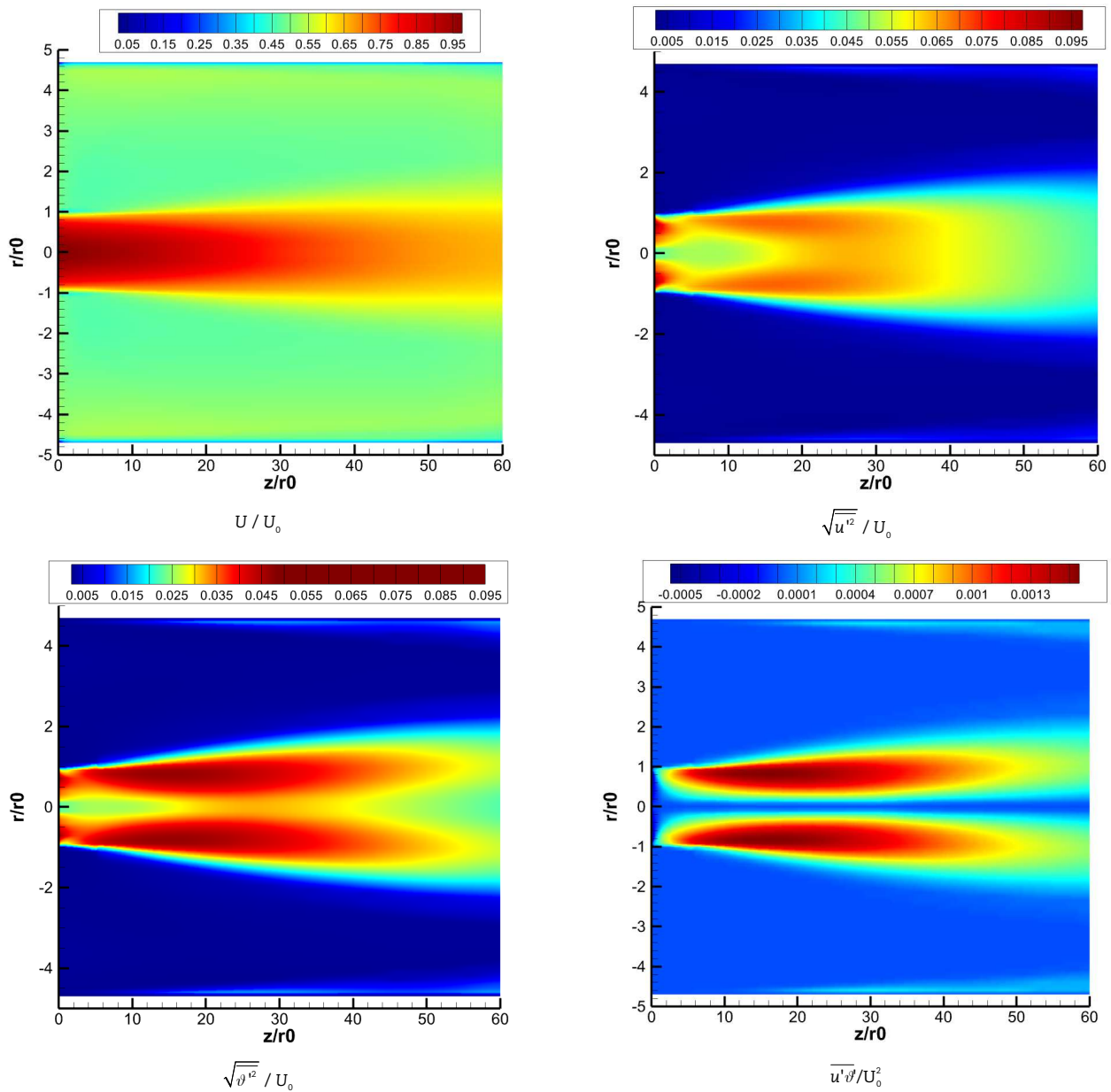


Fig. 12. Contours for averaged axial, fluctuating velocities and turbulent air stress.



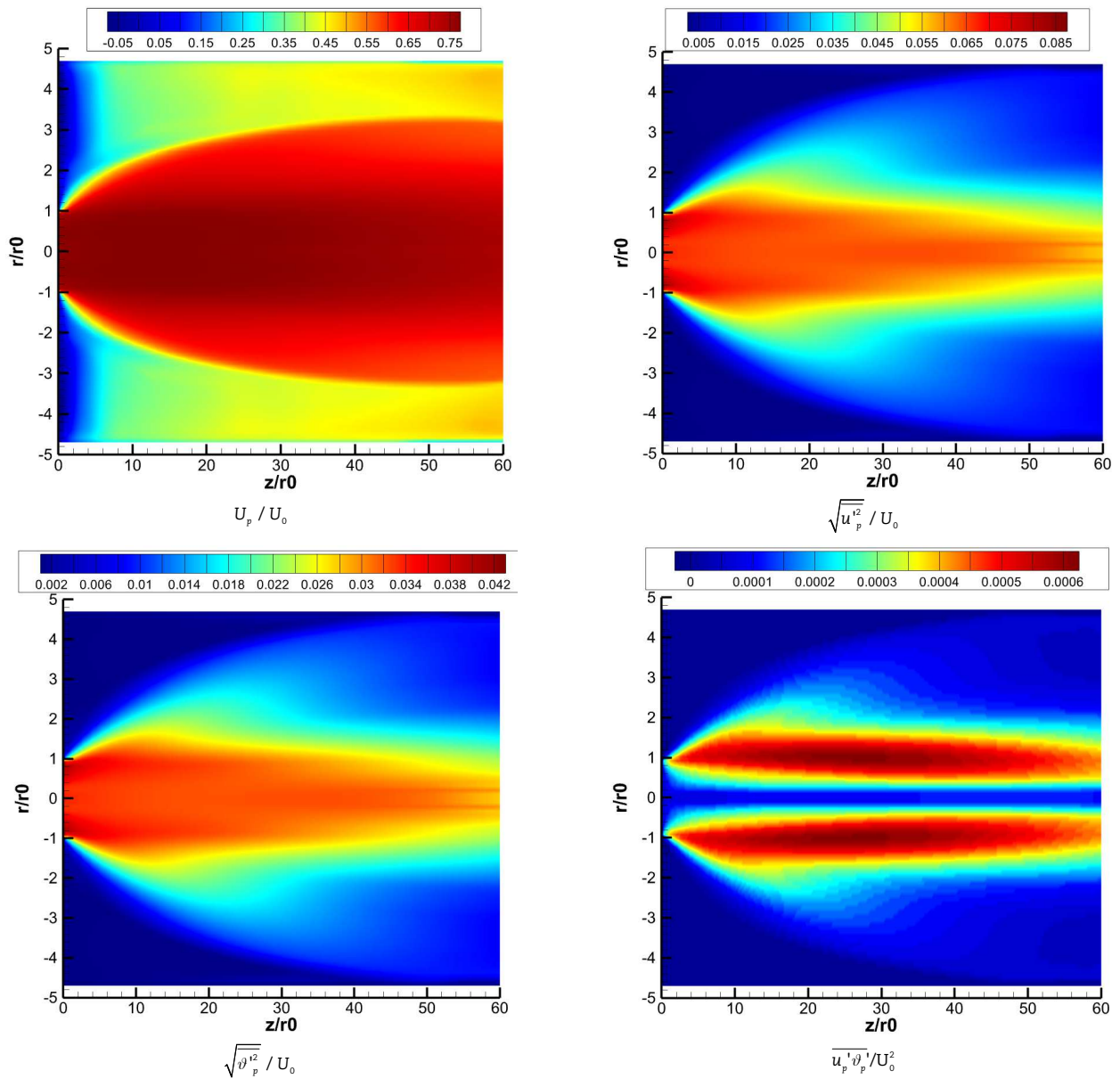


Fig. 13. Contours for averaged axial, fluctuating velocities and turbulent stress for the solid phase.

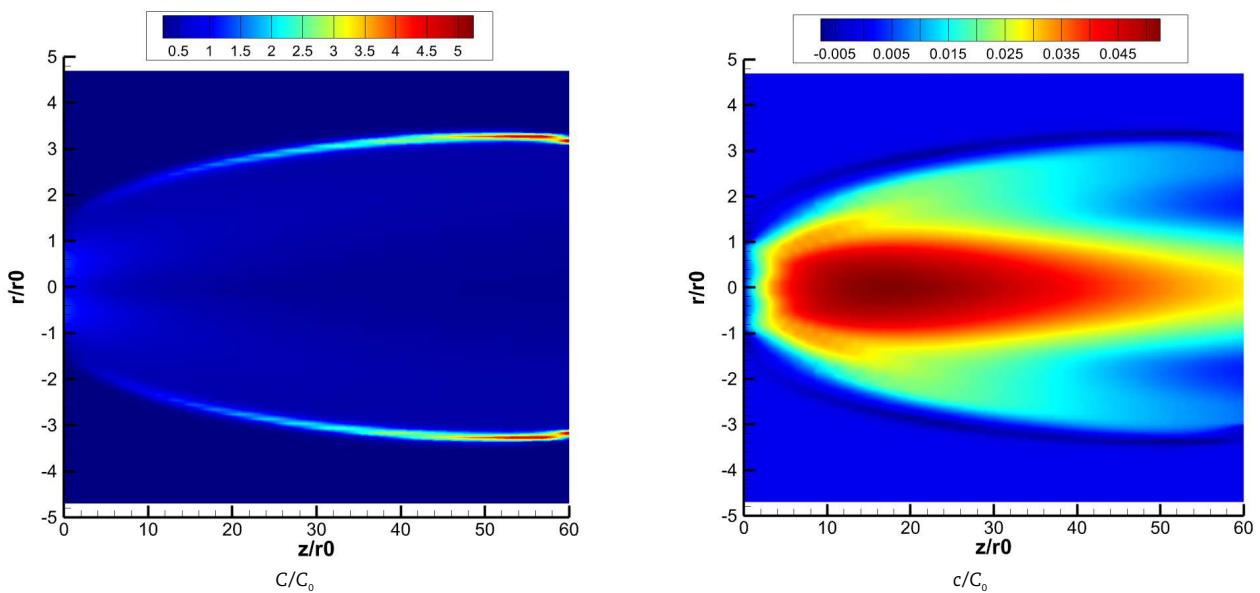


Fig. 14. Isoline of distribution of concentration and fluctuations of particle concentration.



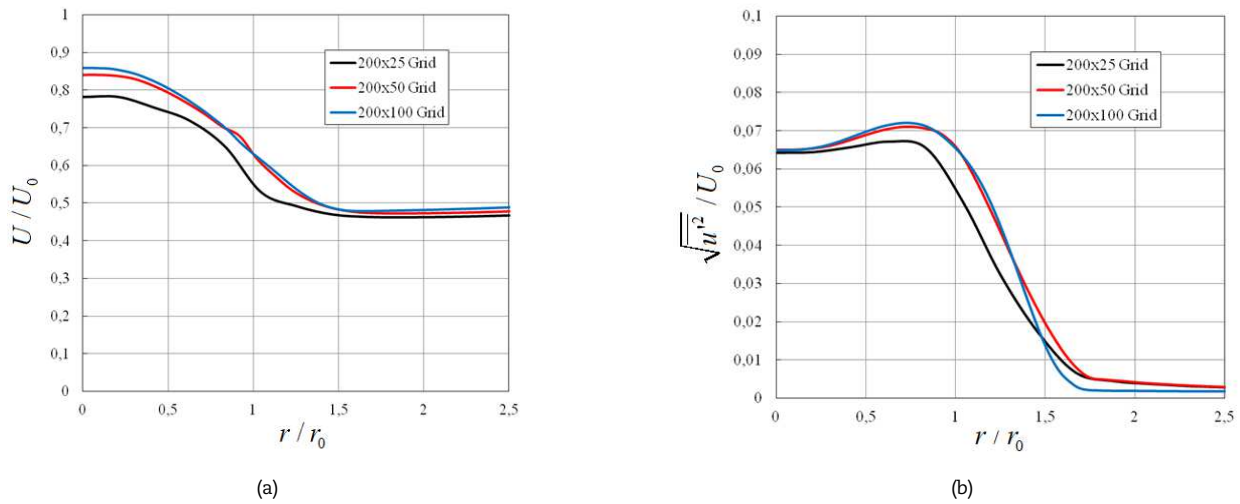


Fig. 15. Effect of changing the calculation node on the result; (a) axial flow velocity, (b) axial fluctuating velocity.

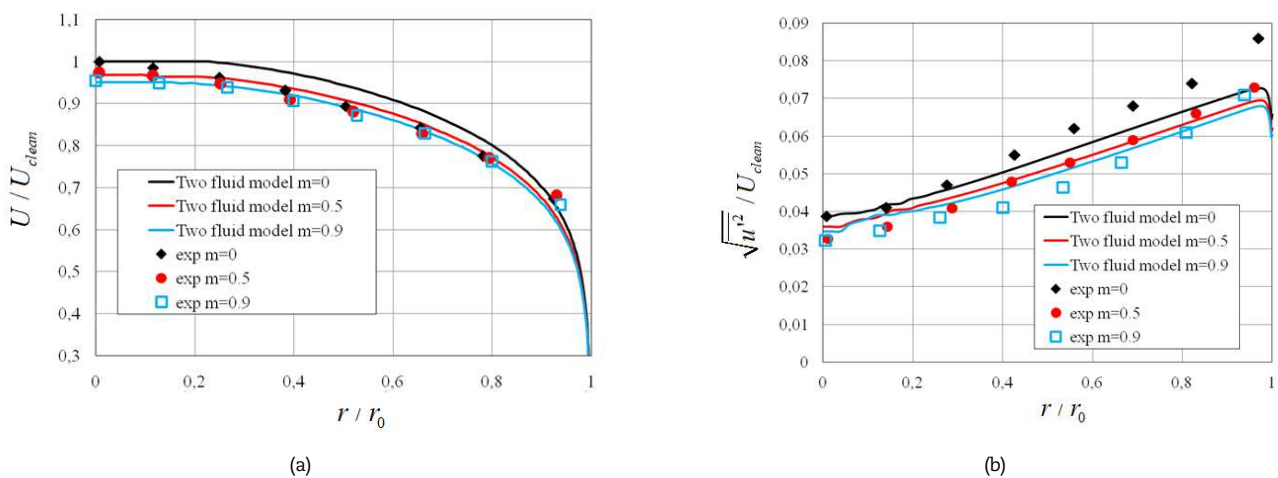


Fig. 16. Profiles of averaged and fluctuating air flow velocities with small particles.

To check the grid convergence, Fig. 15 shows the results for three computational grids (1 - 200x25, 2 - 200x50 and 3 - 200x100) at $x/d = 10$. The calculation grid step in the radial direction for the 200x25 grid is $\Delta r = 0.18$, for the 200x50 grid - $\Delta r = 0.09$ and for the 200x100 grid - $\Delta r = 0.045$.

As can be seen from Fig. 15, the calculation results remain unchanged after the number of nodes exceeds 200x50. This indicates that further increasing the mesh density does not have a significant effect on the simulation results. Thus, we can conclude that the 200x50 grid is sufficiently accurate for calculating axisymmetric jet flows, and further increasing the number of nodes does not improve the accuracy of the results.

6. Vertical Two-Phase Flow in a Pipe

Many researchers have studied two-phase flow. For example, Tsuji et al. [26] experimentally studied upward turbulent two-phase flow (gas + solids) in a pipe. Using laser Doppler velocity, they obtained results primarily for averaged axial and root mean square air velocities at various Reynolds numbers, mass loads, and particle diameters. The pipe diameter was 30.5 mm, and the experimental results were obtained at a height of $x = 5.1$ m above the inlet, i.e., completely in developed turbulent flow. In this work, the study was carried out with small polystyrene particles at mass loads of 0.5, 0.9 and 1.3 s (average diameter 243 μm , $\rho_p = 1020$ kg/m^3) and large particles with mass load 0.6 (average diameter 1420 μm , $\rho_p = 1020$ kg/m^3) [19]. The air velocity on the axis was equal to $U_{clean} = 13.4$ m/s.

When modeling the problem, a computational grid of 200x100 was used. At the inlet, a uniform profile of the longitudinal velocity of the gas and for the solid phase was set, the transverse component of the velocity and pressure were equal to zero, and the relative velocities were also equal to zero. At the exit from the channel, extrapolation conditions of the second order of accuracy were specified for all parameters. To reduce the equations to dimensionless form, all velocities are related to the air flow velocity on the axis of the U_{clean} pipe, and all distances are related to the nozzle radius $r_0 = d/2$.

Figure 16 presents the results of numerical simulations based on the new approach and experimental data for small particles at various values of the particle mass load. Similar results for larger particles are presented in Fig. 17.

From Figs. 15 and 16, it is clear that the results of the proposed mathematical model are in satisfactory agreement with the experimental data. Table 3 shows the results shown in Fig. 17 along with the table and relative error.



Table 3. The relative error of two fluid mathematical model.

r/r_0	$m = 0$			$m = 0.6$			$m = 0$			$m = 0.6$		
	U / U_{clean}	exp	δ	U / U_{clean}	exp	δ	$\sqrt{u'^2} / U_{clean}$	exp	δ	$\sqrt{u'^2} / U_{clean}$	exp	δ
0	1,001582	0,996661	0,492096	1,013884	1,002812	1,107205	0,037742	0,037742	0	0,051362	0,051254	0,010753
0.1	1,002812	0,980668	2,214414	1,012654	1,000351	1,230229	0,040251	0,040251	0	0,051183	0,051971	0,078853
0.2	1,001582	0,965905	3,567668	1,011424	0,984358	2,706507	0,043656	0,043656	0	0,052437	0,053262	0,082437
0.3	0,99051	0,951142	3,936727	0,996661	0,963445	3,321614	0,046882	0,048315	0,14337	0,05405	0,054552	0,050178
0.4	0,974517	0,930228	4,42882	0,979438	0,943761	3,567664	0,050466	0,053154	0,268817	0,056201	0,054409	0,179211
0.5	0,946221	0,901933	4,428822	0,953603	0,928998	2,460458	0,054588	0,057993	0,340502	0,059606	0,056559	0,304659
0.6	0,909315	0,862566	4,674867	0,920387	0,900703	1,968367	0,058351	0,062652	0,430107	0,063548	0,061147	0,240143
0.7	0,865026	0,815817	4,920916	0,872408	0,846573	2,583479	0,062473	0,06767	0,519712	0,06767	0,064301	0,336917
0.8	0,801054	0,760457	4,059755	0,809666	0,789982	1,968367	0,066416	0,071792	0,537634	0,071613	0,064301	0,731183
0.9	0,701406	0,7036	0,219405	0,7112	0,727241	1,604077	0,070538	0,075914	0,537634	0,075914	0,066738	0,917563

From Table 3, it can be seen that the relative error of the two-fluid model at mass fraction $m = 0$ is 3.29% and 2.25% at $m = 0.6$. For the root-mean-square fluctuating velocity, the error is 0.27% at $m = 0$ and 0.0575 at $m = 0.6$.

In the work of Alajbegovic et al. [28], a two-phase flow (liquid + solid phase) was experimentally studied. The experiment was carried out in a pipe with a diameter of 30.6 mm, the particle diameter was 2.32 mm, the average volume fraction of the solid phase was $a_p = 2.73 \times 10^{-2}$. A diagram of the experimental setup for a developed liquid-solid flow in a pipe is shown in Fig. 18. To analyze the radial profiles of the flow properties, the results were obtained at a distance of 2.1 m from the inlet.

In this work, the results were obtained at liquid mass flow rates of 1.095, 1.469 and 1.723 kg/s. The solid phase consisted of ceramic particles with an average diameter of 2.32 mm, density $\rho_p = 2540 \text{ kg/m}^3$, the density of the liquid was equal to $\rho_l = 1020 \text{ kg/m}^3$. Figures 19 and 21 show a comparison of model results with experimental data at various fluid flow rates.

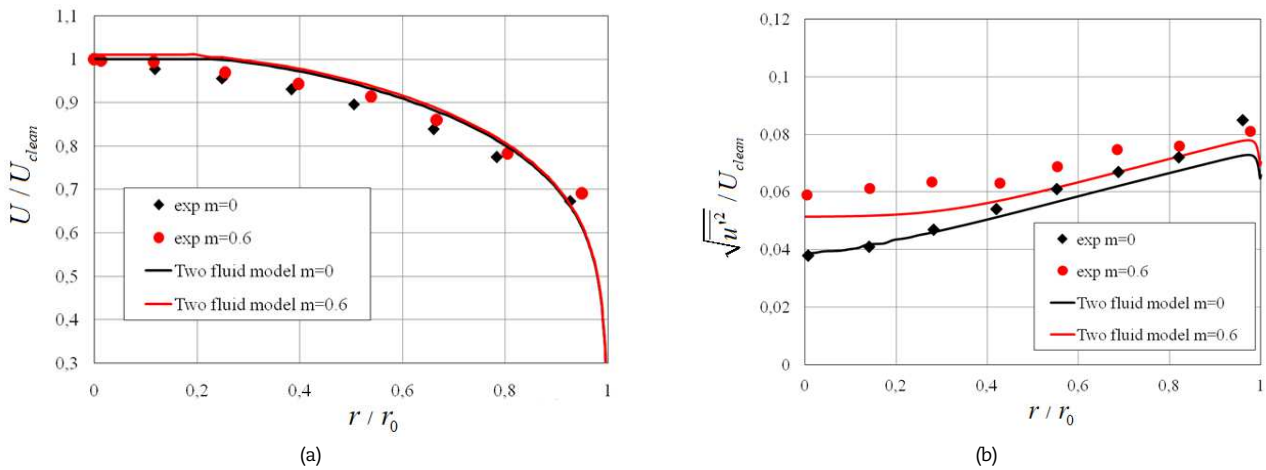


Fig. 17. Profiles of averaged and fluctuating air flow velocities with large particles.

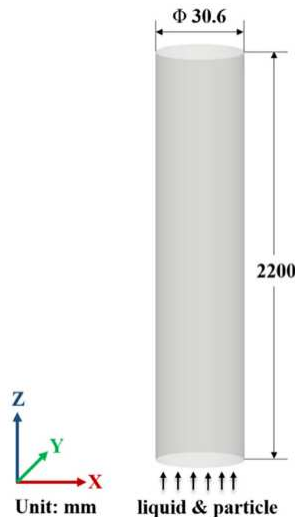


Fig. 18. Sketch of the vertical flow configuration in the pipe by Alajbegovic et al. [28].



From Figs. 19 to 21, it is clear that the model results are in satisfactory agreement with the experimental data. Table 4 shows the relative errors of flow velocity, fluctuations, particle velocity and their fluctuations at a mass fraction of 1.469, kg/s (Fig. 20).

From Table 4, it can be seen that the speed U has a relative error of 0.75%. The root mean square values of fluctuations in flow velocity $\sqrt{u'^2}$, $\sqrt{v'^2}$ and $\overline{u'v'}$ have relative errors of 0.91%, 0.2% and 0.091%, respectively. The particle velocity U_p shows a relative error of 2.44%. Particle velocity fluctuations $\sqrt{u_p'^2}$, $\sqrt{v_p'^2}$ and $\overline{u_p'v_p'}$ have relative errors of 0.91%, 0.2% and 0.91%, respectively.

When studying multiphase flows, the distribution of solid phase concentrations is of great interest. Therefore, Fig. 22 shows the distribution of the concentration of particles with density $\rho_p = 1020 \text{ kg/m}^3$ in the pipe depending on their diameters.

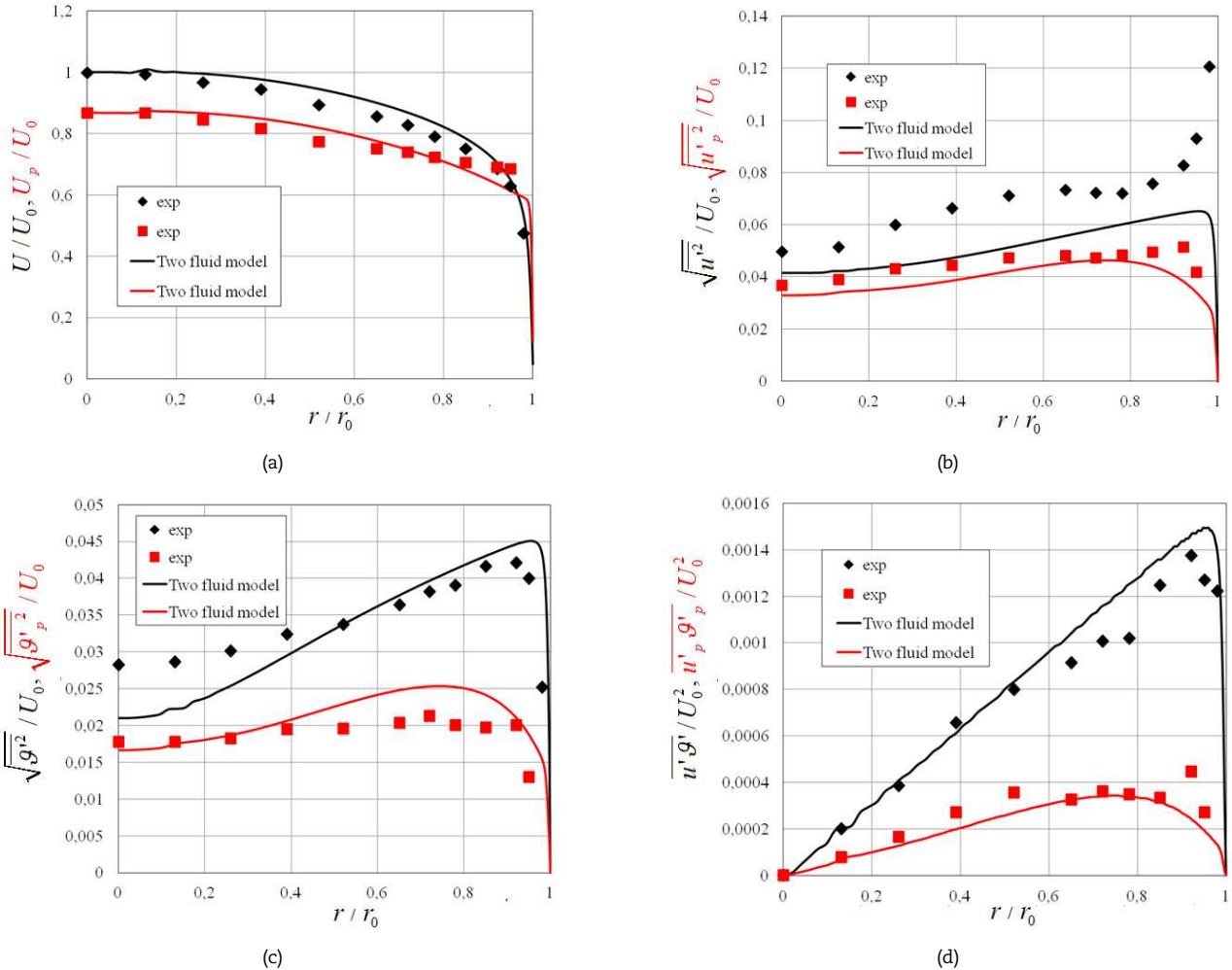


Fig. 19. Comparison of numerical results with experimental data. (a) axial velocity of the liquid and particle; (b) fluctuating axial velocity liquid and particle; (c) fluctuating radial velocity liquid and particle; (d) turbulent stresses at a liquid and particle mass flow rate of 1.095, kg/s.

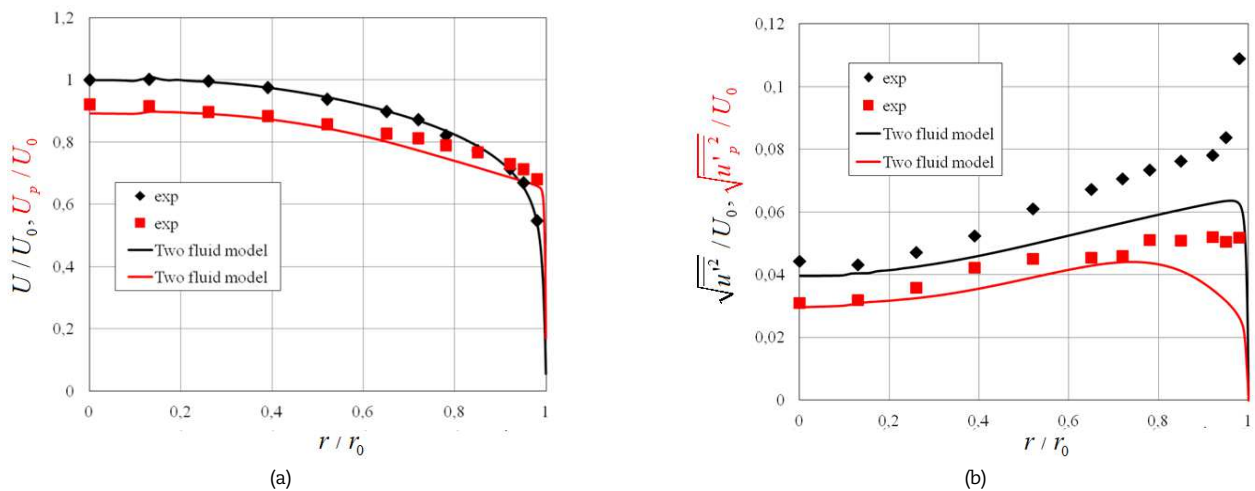


Fig. 20. Comparison of numerical results with experimental data. (a) axial velocity of the liquid and particle; (b) fluctuating axial velocity liquid and particle; (c) fluctuating radial velocity liquid and particle; (d) turbulent stresses at a liquid and particle mass flow rate of 1.469, kg/s.



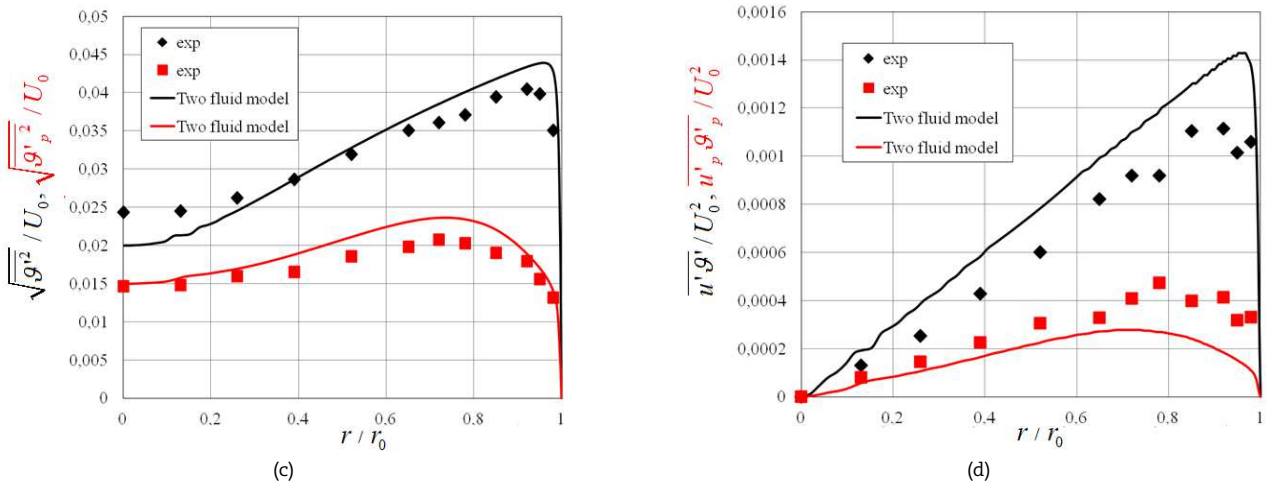


Fig. 20. Continued.

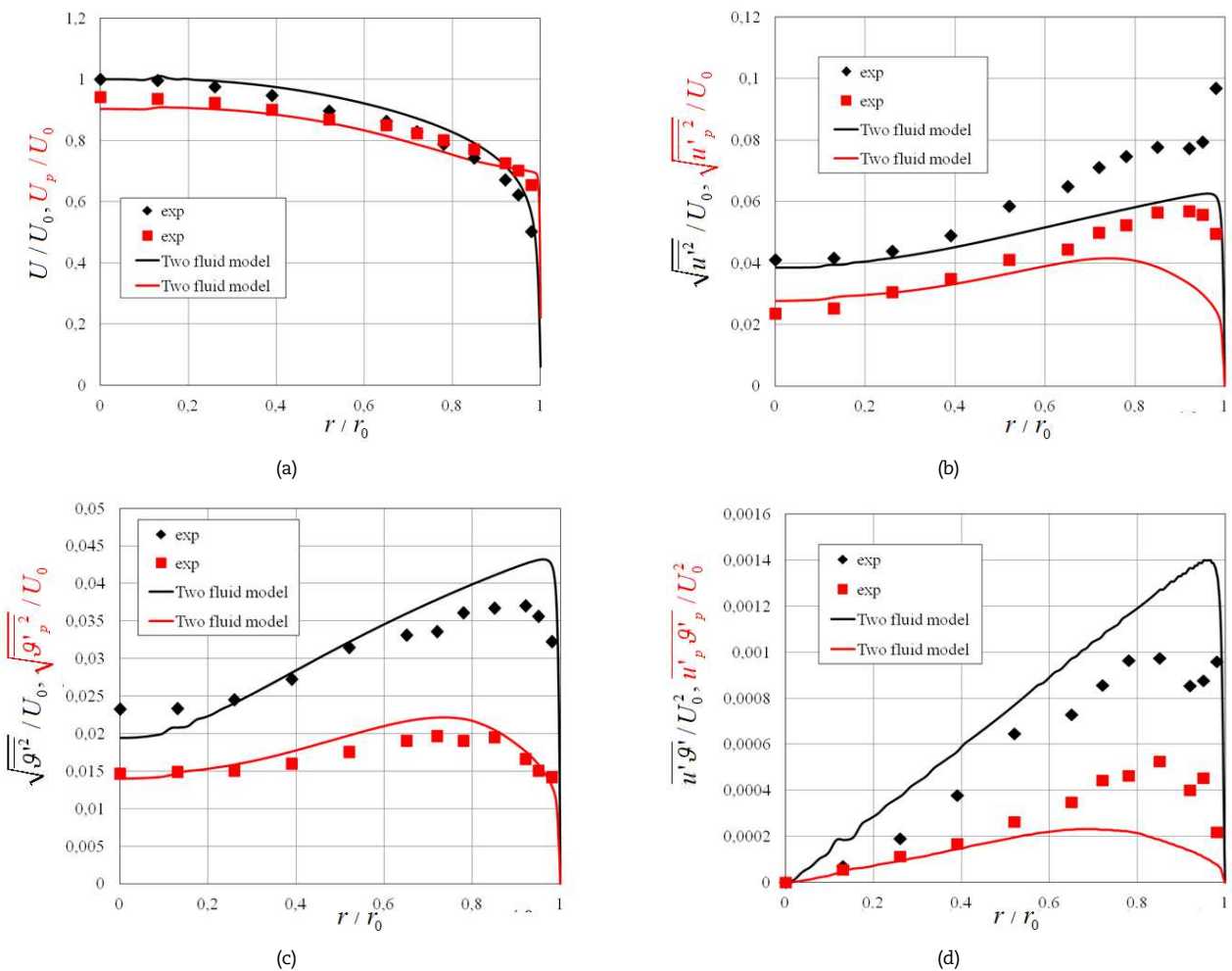


Fig. 21. Comparison of numerical results with experimental data. (a) axial velocity of the liquid and particle; (b) fluctuating axial velocity liquid and particle; (c) fluctuating radial velocity liquid and particle; (d) turbulent stresses at a liquid and particle mass flow rate of 1.723, kg/s.

As can be seen from Fig. 22, the radial distribution of particle concentration is almost uniform with a particle diameter of 5-10 μm . With a particle diameter of 100-250 microns, it is clear that the accumulation of particles occurs near the wall and axis of the pipe. This phenomenon is known as turbulent particle migration [30]. As can be seen, the proposed model is able to adequately describe this phenomenon. It is also clear from the presented figure that for large particles this phenomenon does not manifest itself due to the inertia of the particles. Figure 23 shows the concentration distribution depending on the density of particles with a diameter of $d = 250 \mu\text{m}$.

Figure 24 shows the effect of changing the computational mesh on the result. There are 4 different sets of calculations used here: 1-200x25, 2-200x50, 3-200x100 and 4-200x200. The results obtained show that particles in the pipe mainly accumulate near the axis, and in the jet far from the axis. As can be seen from Fig. 24, the change in the result is very small when the computational mesh exceeds 200x100.



Table 4. Relative errors of flow velocity, mean square fluctuation, turbulent stresses, particle velocity, mean square fluctuation and turbulent stresses.

Flow rate, mean square fluctuation and turbulent stresses												
r/r_0	U	exp	δ	$\sqrt{u'^2}$	exp	δ	$\sqrt{v'^2}$	exp	δ	$\overline{u'v'}$	exp	δ
0	0,959571	0,968157	0,858672	0,039464	0,044821	0,535715	0,019888	0,024201	0,431226	-8,35E-07	-8,35E-07	0
1	0,959571	0,966011	0,644007	0,039464	0,04375	0,428572	0,020706	0,024498	0,379182	0,000124	9,44E-05	0,003006
2	0,957424	0,970304	1,288016	0,041071	0,044821	0,375	0,022937	0,025019	0,208178	0,000302	0,000197	0,010522
3	0,94669	0,955277	0,858681	0,043393	0,048214	0,482144	0,025762	0,026877	0,111524	0,000445	0,000315	0,013027
4	0,92737	0,935957	0,858672	0,045893	0,0525	0,660714	0,028736	0,029257	0,052045	0,000595	0,000435	0,016033
5	0,90161	0,90161	0	0,048929	0,059643	1,071429	0,032007	0,031933	0,007435	0,000743	0,000553	0,01904
6	0,86297	0,860823	0,214666	0,052679	0,065	1,232143	0,035204	0,034312	0,089219	0,000916	0,000743	0,017286
7	0,813596	0,809302	0,429332	0,055714	0,069286	1,357142	0,03803	0,036097	0,193309	0,001059	0,000899	0,016033
8	0,759928	0,742755	1,717345	0,058571	0,073929	1,535714	0,040558	0,037361	0,319702	0,001222	0,001006	0,021545
9	0,644007	0,637567	0,64401	0,062321	0,076964	1,464286	0,04316	0,040186	0,297398	0,001354	0,001116	0,0238

Particle velocity and mean square fluctuation and turbulent stresses												
r/r_0	U_p	exp	δ	$\sqrt{u_p'^2}$	exp	δ	$\sqrt{v_p'^2}$	exp	δ	$\overline{u_p'v_p'}$	exp	δ
0	0,835063	0,860823	2,576038	0,039464	0,044821	0,535715	0,01461	0,014461	0,014871	6,68E-06	0	0,000668
1	0,828623	0,858676	3,005364	0,039464	0,04375	0,428572	0,015279	0,014833	0,04461	3,67E-05	6,93E-05	0,003257
2	0,832916	0,845796	1,288007	0,041071	0,044821	0,375	0,016171	0,015353	0,081784	8,94E-05	0,000119	0,003006
3	0,828623	0,835063	0,643997	0,043393	0,048214	0,482144	0,017584	0,016022	0,156134	0,000124	0,000185	0,006013
4	0,802862	0,824329	2,146694	0,045893	0,0525	0,660714	0,018848	0,016543	0,230483	0,000172	0,000232	0,006013
5	0,779249	0,794275	1,502685	0,048929	0,059643	1,071429	0,021004	0,01803	0,297398	0,000225	0,000297	0,007265
6	0,751342	0,755635	0,429338	0,052679	0,065	1,232143	0,022416	0,019591	0,282528	0,000257	0,00032	0,006263
7	0,704115	0,734168	3,005364	0,055714	0,069286	1,357142	0,023532	0,020409	0,312268	0,000285	0,000403	0,011775
8	0,646154	0,695528	4,93738	0,058571	0,073929	1,535714	0,023086	0,01974	0,334572	0,000265	0,000458	0,01929
9	0,592487	0,64186	4,93738	0,062321	0,076964	1,464286	0,020112	0,017509	0,260223	0,000207	0,000408	0,020042

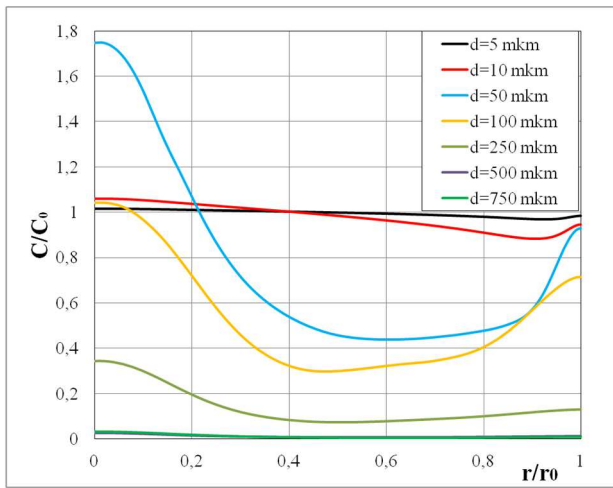


Fig. 22. Distribution of particle concentration in a pipe depending on their diameters.

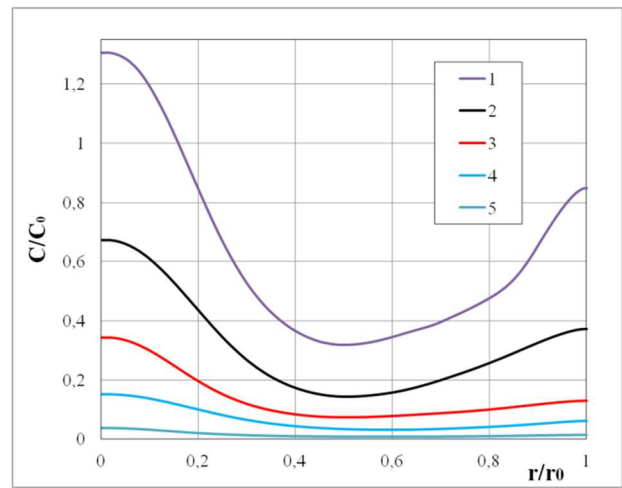


Fig. 23. Distribution of particles with a diameter of $d = 250$ microns at different densities.

Here 1 - $\rho_p = 100 \text{ kg/m}^3$, 2 - $\rho_p = 500 \text{ kg/m}^3$, 3 - $\rho_p = 1000 \text{ kg/m}^3$,
 4 - $\rho_p = 2000 \text{ kg/m}^3$, 5 - $\rho_p = 3000 \text{ kg/m}^3$

7. Conclusion

In this work, a mathematical model of a two-phase turbulent flow based on a two-fluid approach was obtained. It was shown that the two-fluid approach to turbulence leads to a closed system of equations and was an effective approach in the study of complex hydrodynamic systems. The results of the analysis carried out on the basis of this approach allow us to obtain a deep understanding of the behavior of various parameters of two-phase flows, such as velocity fluctuations, interactions between phases, etc. It was also shown that the results of the proposed model were in good agreement with experimental data, and the model adequately describes such a complex phenomenon such as turbulent migration of particles. Thus, modeling of turbulent two-phase flow based on the two-fluid approach is an effective tool for scientific and engineering research, as well as for the development and optimization of various technical systems in which moving fluids play an important role.



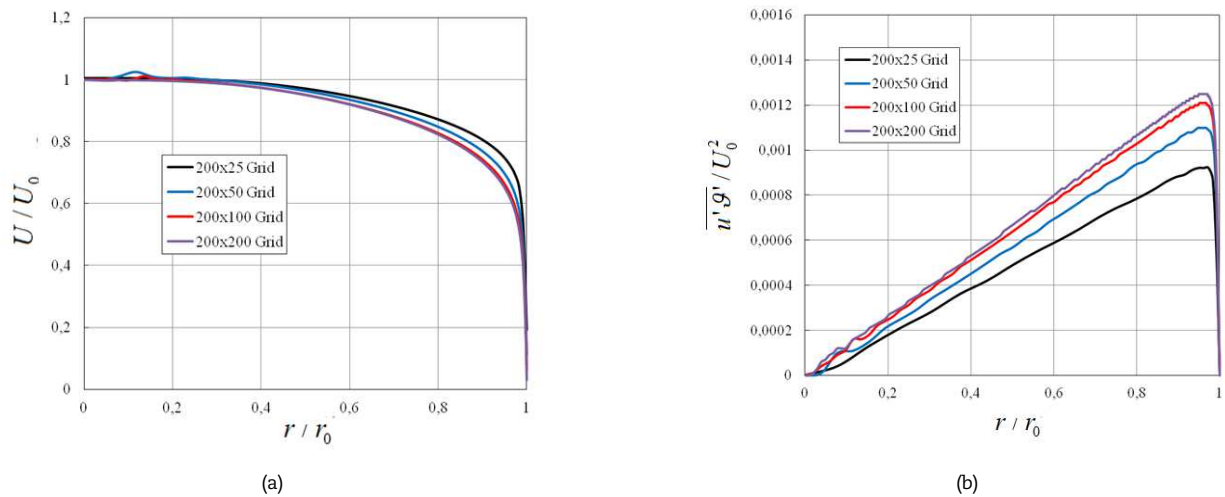


Fig. 24. Changing the calculation grid affects the result; (a) axial velocity of the liquid, (b) turbulent stresses at a liquid.

Author Contributions

Z.M. Malikov: Writing (first draft), Writing the first draft, writing a review. M.E. Madaliev: Formal analysis, data processing, data collection, first draft writing. The manuscript was written through the contribution of all authors. All authors discussed the results, reviewed, and approved the final version of the manuscript.

Acknowledgments

Not applicable.

Conflict of Interest

The authors confirmed that they have no competing financial interests or personal relations that could influence the work presented in the paper.

Funding

The authors received no financial support for the research, authorship, and publication of this article.

Data Availability Statements

The datasets generated and/or analyzed during the current study are available from the corresponding author on reasonable request.

Nomenclature

V_i	Component of the average flow velocity [m/s]	V_{pi}	Component of the average particle velocity [m/s]
ϑ_i	Component of the relative velocity [m/s]	ϑ_{pi}	Component of the relative velocity particle [m/s]
C	Mass concentration of solid phase	c	Relative solids concentration
ν_{β}	Effective kinematic viscosity tensor arising from the relative motion of fluids [m ² /s]	p	Pressure in fluid mixture [Pa]
K_f	Scalar function of the friction force [1/s]	C_s	Shear coefficient
ν	Molecular viscosity [m ² /s]	t	Time [s]
τ_p	Interaction relaxation time [s]	C_{f1}	First constant in the coefficient of friction
C_{f2}	Second constant in the coefficient of friction	λ_{max}	Largest root of the characteristic equation [1/s]
S_y	Strain rate tensor of a mixture of fluids	Re	Reynolds number
Re_p	Reynolds number for particles	d	Nearest dist. from a given point to a solid wall [m]
ρ	Density [kg/m ³]	c_d	Drag coefficient


References


- [1] Kohnen, G., Sommerfeld, M., The effect of turbulence modeling on turbulence modification in two-phase flows using the Euler-Lagrange approach, *Symposium on Turbulent Shear Flows*, 11 th, Grenoble, France, 1997.
- [2] Squires, K.D., Eaton, J.K., On the modeling of particle-laden turbulent flows, *Proceedings of the Sixth Workshop on Two-Phase Flow Predictions*, Erlangen, Germany, 1992.
- [3] Lun, C.K.K., Numerical simulation of dilute turbulent gas–solid flows, *International Journal of Multiphase Flow*, 26(10), 2000, 1707–1736.
- [4] Zhou, M., Wang, S., Kuang, S., Luo, K., Fan, J., Yu, A., CFD-DEM modelling of hydraulic conveying of solid particles in a vertical pipe, *Powder Technology*, 354, 2019, 893–905.
- [5] Xu, L., Zhang, Q., Zheng, J., Zhao, Y., Numerical prediction of erosion in elbow based on CFD-DEM simulation, *Powder Technology*, 302, 2016, 236–



- 246.
- [6] Kuang, S.B., Li, K., Zou, R.P., Pan, R.H., Yu, A.B., Application of periodic boundary conditions to CFD-DEM simulation of gas–solid flow in pneumatic conveying, *Chemical Engineering Science*, 93, 2013, 214–228.
- [7] Gui, N., Fan, J.R., Luo, K., DEM–LES study of 3-D bubbling fluidized bed with immersed tubes, *Chemical Engineering Science*, 63(14), 2008, 3654–3663.
- [8] Moukalled, F., Mangani, L., Darwish, M., *Introduction BT - The Finite Volume Method in Computational Fluid Dynamics: An Advanced Introduction with OpenFOAM® and Matlab*, F. Moukalled, L. Mangani, and M. Darwish, Eds., Cham: Springer International Publishing, 2016, doi: 10.1007/978-3-319-16874-6_1.
- [9] Zhang, H., Ahmadi, G., Aerosol particle transport and deposition in vertical and horizontal turbulent duct flows, *Journal of Fluid Mechanics*, 406, 2000, 55–80.
- [10] Yu, K.F., Lau, K.S., Chan, C.K., Numerical simulation of gas-particle flow in a single-side backward-facing step flow, *Journal of Computational and Applied Mathematics*, 163(1), 2004, 319–331.
- [11] Fessler, J.R., Eaton, J.K., Turbulence modification by particles in a backward-facing step flow, *Journal of Fluid Mechanics*, 394, 1999, 97–117.
- [12] Melville, W.K., Bray, K.N.C., A model of the two-phase turbulent jet, *International Journal of Heat and Mass Transfer*, 22(5), 1979, 647–656.
- [13] Rizk, M.A., Elghobashi, S.E., A two-equation turbulence model for dispersed dilute confined two-phase flows, *International Journal of Multiphase Flow*, 15(1), 1989, 119–133.
- [14] Al Taweel, A.M., Landau, J., Turbulence modulation in two-phase jets, *International Journal of Multiphase Flow*, 3(4), 1977, 341–351.
- [15] Sun, T.Y., Faeth, G.M., Structure of turbulent bubbly jets—II. Phase property profiles, *International Journal of Multiphase Flow*, 12(1), 1986, 115–126.
- [16] Muyschondt, A., Anand, N.K., McFarland, A.R., Turbulent deposition of aerosol particles in large transport tubes, *Aerosol Science and Technology*, 24(2), 1996, 107–116.
- [17] Crowe, C.T., On models for turbulence modulation in fluid–particle flows, *International Journal of Multiphase Flow*, 26(5), 2000, 719–727.
- [18] Crowe, C.T., Turbulence modulation of fluid-particle flows-A basic approach, *3rd Int. Conf. Multiphase Flows*, 1998.
- [19] Lain, S., Sommerfeld, M., Turbulence modulation in dispersed two-phase flow laden with solids from a Lagrangian perspective, *International Journal of Multiphase Flow*, 24(4), 2003, 616–25.
- [20] Boulet, P., Moissette, S., Influence of the particle-turbulence modulation modelling in the simulation of a non-isothermal gas–solid flow, *International Journal of Heat and Mass Transfer*, 45(20), 2002, 4201–4216.
- [21] Malikov, Z., Mathematical model of turbulence based on the dynamics of two fluids, *Applied Mathematical Modelling*, 82, 2020, 409–436.
- [22] Hishida, K., Turbulence characteristics of gas-solids two-phase confined jet (effect of particle density), *Japanese Society for Multiphase Flow*, 1(1), 1987, 56–69.
- [23] Hishida, K., Umemura, K., Maeda, M., Heat transfer to plane wall jet in gas-solids two-phase flow, *International Heat Transfer Conference Digital Library*, Begel House Inc., 1986.
- [24] Hishida, K., Nakano, H., Maeda, M., Turbulent Flow Characteristics of Liquid-Solid Particle Confined Jet, *International Conference on Mechanics of Two-Phase Flows*, 1989.
- [25] Hishida, K., Nakano, H., Fujishiro, T., Maeda, M., Turbulence characteristics of liquid-solids two-phase circular confined jet, *Transactions of the JSME*, 55, 1989, 648–654.
- [26] Tsuji, Y., Morikawa, Y., Shiomi, H., LDV measurements of an air-solid two-phase flow in a vertical pipe, *Journal of Fluid Mechanics*, 139, 1984, 417–434.
- [27] Tsuji, Y., Morikawa, Y., LDV measurements of an air–solid two-phase flow in a horizontal pipe, *Journal of Fluid Mechanics*, 120, 1982, 385–409.
- [28] Alajbegovic, A., Assad, A., Bonetto, F., Lahey Jr, R.T., Phase distribution and turbulence structure for solid/fluid upflow in a pipe, *International Journal of Multiphase Flow*, 20(3), 1994, 453–479.
- [29] Malikov, Z.M., Modeling a turbulent multicomponent fluid with variable density using a two-fluid approach, *Applied Mathematical Modelling*, 104, 2022, 34–49.
- [30] Mednikov, E.P., *Turbulent Transport and Deposition of Aerosols*, Nauka, Moscow, 1980.
- [31] Patankar, S., *Numerical heat transfer and fluid flow*, Taylor & Francis, 2018.

ORCID iD

Z.M. Malikov  <https://orcid.org/0000-0001-9038-5407>

M.E. Madaliev  <https://orcid.org/0000-0001-9994-8907>



© 2024 Shahid Chamran University of Ahvaz, Ahvaz, Iran. This article is an open access article distributed under the terms and conditions of the Creative Commons Attribution-NonCommercial 4.0 International (CC BY-NC 4.0 license) (<http://creativecommons.org/licenses/by-nc/4.0/>).

How to cite this article: Malikov Z.M., Madaliev M.E. Modeling of Turbulent Two-Phase Flow based on a Two-Fluid Approach, *J. Appl. Comput. Mech.*, xx(x), 2024, 1–19. <https://doi.org/10.22055/jacm.2024.46940.4632>

Publisher's Note Shahid Chamran University of Ahvaz remains neutral with regard to jurisdictional claims in published maps and institutional affiliations.

